REPUBLIC OF TURKEY

ALTINBAŞ UNIVERSITY

Institute of Graduate Studies

Mechanical Engineering

INVESTIGATION OF THE EFFECTIVE FACTORS ON SOLAR POWERED FIXED-WING UAV FOR EXTENDED FLIGHT ENDURANCE

Aws Tariq Salih AL-FALAHI

Master's Thesis

Supervisor

Asst. Prof. Dr. Yaser ALAIWI

Istanbul, 2022

INVESTIGATION OF THE EFFECTIVE FACTORS ON SOLAR POWERED FIXED-WING UAV FOR EXTENDED FLIGHT ENDURANCE

Aws Tariq Salih AL-FALAHI

Mechanical Engineering

Master's Thesis

ALTINBAŞ UNIVERSITY

2022

The thesis titled INVESTIGATION OF THE EFFECTIVE FACTORS ON SOLAR POWERED FIXED-WING UAV FOR EXTENDED FLIGHT ENDURANCE prepared by AWS TARIQ SALIH AL-FALAHI and submitted on 18/08/2022 has been **accepted unanimously** for the degree of Master of Science in Mechanical Engineering.

Asst. Prof. Dr. Yaser ALAIWI

Supervisor

Thesis Defense Committee Members:

Asst. Prof. Dr. Yaser ALAIWI	Faculty of Engineering and Architecture, Altınbaş University	_____
Asst. Prof. Dr. Hakan KAYGUSUZ	Faculty of Engineering and Architecture, Altınbaş University	_____
Assoc. Prof. Dr. Haydar İzzettin KEPEKÇİ	Faculty of Engineering and Architecture, Nişantaşı University	_____

I hereby declare that this thesis meets all format and submission requirements of a Master's thesis.

Submission date of the thesis to Institute of Graduate Studies: ___/___/___

I hereby declare that all information/data presented in this graduation project has been obtained in full accordance with academic rules and ethical conduct. I also declare all unoriginal materials and conclusions have been cited in the text and all references mentioned in the Reference List have been cited in the text, and vice versa as required by the abovementioned rules and conduct.

Aws Tariq Salih Al-Falahi

Signature

DEDICATION

To my lovely father and mother and brother and sisters always respected what I wanted to do and gave me the full support, and encouragement for whole my life. I like to express my greatest appreciation for your enormous love.

ABSTRACT

INVESTIGATION OF THE EFFECTIVE FACTORS ON SOLAR POWERED FIXED-WING UAV FOR EXTENDED FLIGHT ENDURANCE

Al-Falahi, Aws Tariq Salih

M.Sc., Mechanical Engineering, Altınbaş University,

Supervisor: Asst. Prof. Dr. Yaser ALAIWI

Date: 08/2022

Pages: 81

The wing is the most crucial component of the airplane. All other aircraft components are influenced by the wing geometry. Due to airflow characteristics, the form of the geometry has an impact on the airplane forces. Adding solar cells to the aircraft will also improve the flying time characteristics. As a result, the major purpose of this study is to know the changes affecting airfoil properties utilizing various wing shapes. The CFD ANSYS software was used to attain this purpose. NACA 0009 was used to validate the current system. The purpose of selecting this model is to gain a better understanding of the forces' behaviour in relation to subsonic aircraft, allowing the researcher to improve the wing shape design. In this study, several factors were taken into account, beginning with the air speed, which was given as (5.5, 8.8, and 11.11) m/s. Based on the changes in lift and drag coefficients, the simulation results reveal that there is identification between the selected two types of airfoils. Due to the lift force caused by air speed, the lift coefficient and drag coefficient have been discovered. In both situations, the increases are gradual as the angle of attack is increased. The study discovered that when the angle of attack is increased, a drag force increases. The drag force caused a downwash of air behind the wing, posing a serious threat to the plane's lift and stability. To prevent this issue, the current work uses optimal wing design to optimize the wing design. Because the stresses on the top and bottom of the wing are separated in the new recommended wing, the induced drag has been decreased. The

findings of the study increased the airplane's flight duration and decreased its power rating. The results show that lift force, lift coefficient, and drag coefficient all improve wing performance.

Keywords: Fixed-Wing UAV, Wing Performance, S1223, S1223RTL, Solar.

TABLE OF CONTENTS

Pages

LIST OF TABLES

Pages

LIST OF FIGURES

Pages

ABBREVIATIONS

CFD : Computational Fluid Dynamics

ANSYS : Analysis System

UAV : Unmanned Aerial Vehicle

LIST OF SYMBOLS

CL	:	The lift coefficient
CM	:	Moment coefficient
a	:	Angle of attack
b	:	Negative of angle of attack for zero lift
c	:	Length of the airfoil chord
p	:	Pressure
p	:	Position of the maximum camber along the chord
Re	:	Reynolds number
T	:	Fluid temperature
t	:	Maximum airfoil thickness in tenths of chord
v	:	Velocity
x	:	Coordinates along the length of the airfoil
y	:	Coordinates above and below the line
yc	:	Camber coordinates
yt	:	Thickness coordinates

1. INTRODUCTION

Efficiency in aerodynamic design is described as having the lowest drag for a fixed-wing aircraft. Consequently, the best design for a flying wing is the most aerodynamically efficient wing design. The airfoil specification was investigated meticulously to manage the wing development based on the clean flying conceptual design. The geometry of an airfoil as seen in cross-section may be used to calculate design factors such as stabilizer position, aircraft mass, control surface size, and wing surface area. The conventional method for determining the precise solution is to use full Navier- Stokes equations, which are used in challenging cases. Solving these equations is a stand-alone task in the airfoil model [1]. Because of their complexity, the appropriate equations and conditions must be specified based on the flow regime. The ANSYS CFD approach is used to optimize airfoils that are subject to a variety of objectives and restrictions, or it may be used in complex schemes to parameterize complete wings and airplanes [2]. The effect of different airfoil behaviors on the wing design of several aircraft models will be examined in this study.

1.1 BACKGROUND OF STUDY

Aerodynamic design is a hot issue in the aviation industry because it has the potential to enhance aircraft design in a variety of ways, including improved aerodynamic properties and reduced weight. The lift force balance in respect to the plane's weight may be defined using the airfoil's effect. The amount of drag force applied to the aircraft is also important. The growth of airfoil research may be traced back to the 1960s, when technology improved and numerical solutions were available. In the 1970s, aerodynamic shapes were created using 11 distinct factors in a three-dimensional design space. Later techniques got more robust when iterative Computational Fluid Dynamics (CFD) became possible for small-mesh models [3].

The operation type is determined by the performance of the airfoil, which is designed for a certain bearing. It's a critical factor in determining the form and design of a plane's wing during flight. A thick airfoil is more efficient at low speeds, whereas a thin airfoil is more efficient at high speeds. The direct approach and the inverse method are the two basic airfoil design methodologies. To achieve the necessary results, the direct approach employed a well-known airfoil shape with performance comparable to that required by the new application, with minor

adjustments. The inverse technique describes an airfoil's performance parameters and utilizes computer algorithms to create the airfoil shape that accomplishes them [4]. The direct method is straightforward, but the inverse method is significantly more powerful since the designer has far more exact control over the airfoil's eventual performance. Both of these methods are dependent on airfoil design and the effects of lift and drag. The universal Navier-Stokes equations are particularly essential since they account for all possible flow scenarios. However, establishing a numerical solution with them takes a lengthy time. Boundary layer equations might be used to estimate the equations. Outside, viscosity effects may be ignored, and the temperature change of the flow can be considered constant [5].

The wing shape must be researched in order to analyze the airfoil effect on lift and drag forces depending on the wing design. The first step is to determine which wing shape is the most recent and well-known. The National Advisory Committee for Aeronautics is one of the various independent organizations "NACA".They contain information on "airfoil shape families" [6]. The wing shape must be researched in order to evaluate the impact of the airfoil on lift and drag forces based on wing design. The first step is to figure out which wing shape is the newest and most well-known. The "NACA" is one of the various independent bodies (NACA). They go through "airfoil form families" in great depth [7,8].

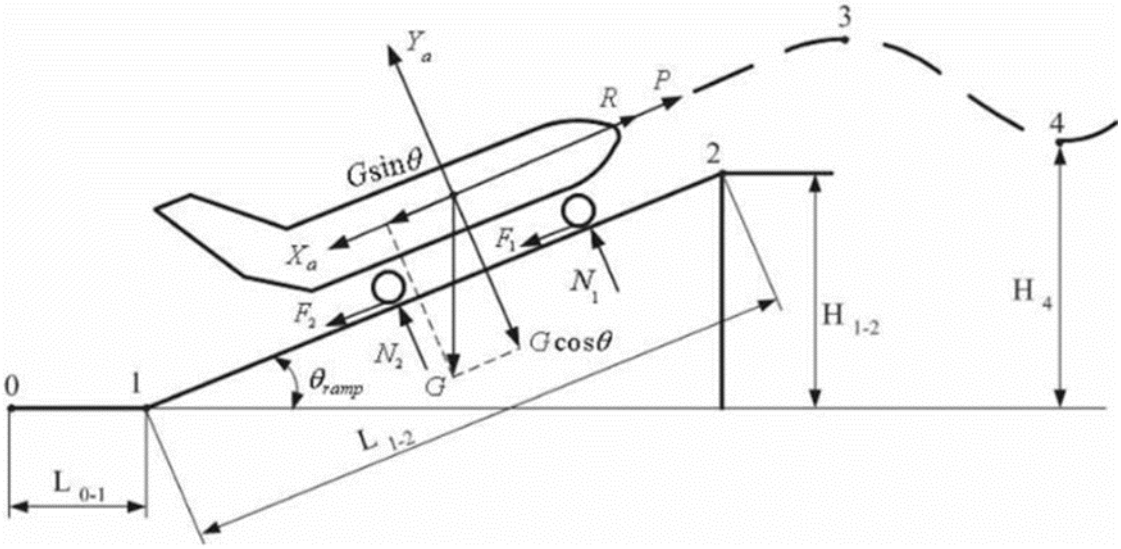

Figure 1.1: Forces on an Airplane in Normal Flight [8].

The flow equations across the boundary layer thickness are comprised of a model for the laminar portion of the flow, a model for the turbulent part of the flow, and a transition criterion.

1.2 PROBLEM STATEMENTS

A wing's lift force and drag are very complex factors of its form. The form and air flow behavior of an item dictate the amount of lift it generates. As a result, in wing design, optimizing the form is a vital case. The intricate interdependence of wing shape, flow conditions, and inclinations may be conveyed using the lift and drag coefficients, which they utilized as the aerodynamic number to express all of the difficult dependencies [9,10]. As a result, the most common method for wing design optimization is to use the lift and drag coefficients from an aerodynamic model. These lift and drag coefficients are related to the wing's operational characteristics, which may be easily translated into performance. A change in the aerodynamic properties of the airfoil, which is determined by the wing design's shape, is the source of this phenomenon. The question is whether the current design can attain optimal lift and drag coefficients with the wings that are now available. To achieve this purpose, the aerodynamic characteristics change may be recognized by studying the differences effect in wing design analysis. This differential effect may be created by modeling the wing using the objective function of an aerodynamic model. The nonlinear problem may be studied using mode simplifications using (CFD) software as a tool [11,12].

1.3 OBJECTIVE OF STUDY

The objectives of the research are:

i. Using CFD software to analyze two types of wings based on lift and drag coefficients.

ii. Study the improved design of chosen wings due to airfoil properties,

iii. Study the solar energy usage as a power resource to optimize the airplane flying time.

1.4 SCOPE OF STUDY

The scopes of this research are:

a) The CFD (Fluent) ANSYS calculation technique was used for the simulation procedure.

b) The first type of airfoil was chosen for validation, while the other two types were chosen for comparison.

c) Determine an acceptable boundary condition for investigating airfoil behavior.

d) To explore airfoil modifications, choose an appropriate angle of attack.

1.5 ORGANIZATION OF THESIS

This dissertation is divided into five chapters. The issue statement, background study, study aim, and research scope are all included in Chapter 1 of this research. The literature review is discussed in Chapter 2. The methodologies and processes employed in Chapter 3 are discussed. The following section shows the research flow chart and planning. The collected results are presented in Chapter 4 and, ultimately, The conclusion and recommendations are included in Chapter 5.

2. LITERATURE REVIEW

There has been a surge in interest in getting an unmanned small aircraft system in recent years. The UAV combines the best features of fixed-wing and rotary-wing aircraft on a single platform, allowing it to take off and land vertically and fly efficiently. Traditional fixed-wing and rotary-wing aircraft cannot offer such capabilities [13]. Unmanned small aircraft systems have become more popular in recent years. The UAV combines the key features of fixed-wing and rotary-wing aircraft on a single platform, allowing it to take off and land vertically and fly efficiently. Traditional fixed-wing and rotary-wing aircraft are unable to offer such capabilities [14]. This chapter teaches aerodynamic concepts based on a variety of airfoil types to help you get started with this subject. The wing configuration designs are discussed in Section 2.2 of this chapter and provide an overview of the various wing configurations. Section 2.3 also discusses the history of airfoils and provides some background information. Section 2.4 explains the fundamentals of aerodynamics, including the wing configuration force analysis method. The concepts of solar energy are discussed in Section 2.5. application in aircraft that allows the researcher to assess the effectiveness of aircraft power consumption The turbulence modeling requirements of the wing design are presented in Section 2,6 in order to describe the ring model specification.

2.1 BACKGROUND OF WING CONFIGURATION DESIGNS

A wing configuration design is a figure shape or appearance of the wing configuration's body. It is divided into two sections. The aircraft's location and number of wing configurations are categorized as first class [15]. The second class is the wing configuration planform. The wing configuration planform has been chosen as the subject of this investigation. The goal of this thesis is to investigate the many forms of flying behaviours and motions that occur throughout a flight [16]. In these circumstances, efficient wing configuration design selection is required to determine the specifications of alternative configuration designs. The aircrafts are designed to perform at their best during the flight stage, which is decided by the aircraft's mission. To enhance the optimal flying envelope, it is essential to be able to identify variations in aerodynamic geometry effect [17]. This is an important objective in aircraft design since it introduces new structural concepts. Various flow conditions perceive different geometries, which means that little adjustments in wing configuration design can have a major influence on

aerodynamic performance [18]. It's vital to understand wing configuration performance and airplane flow characteristics since the wing configuration plan form operates with three dimensions of airflow. Sweepback, taper ratio, and aspect ratio are planform design factors. As a result, as shown in Figure 2.1, identifying these features is crucial in order to investigate the overall aerodynamic.

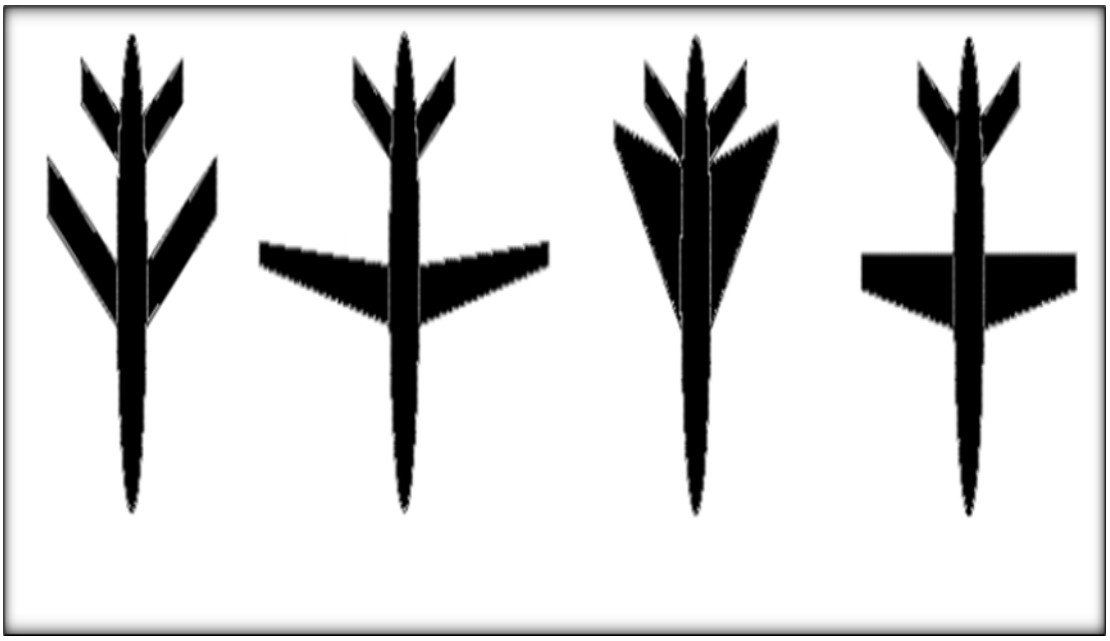

Figure 2.1: Wing Configuration Planform [19].

The first factor (Taper ratio) is defined as the ratio of the tip chord (C_t) to the root chord (R) (C_r). This formula's connection is provided by formula 2.1. The current method may be used to calculate wing configurations as well as vertical and horizontal tails.

$$\lambda = \frac{Ct}{Cr} \qquad 2.1$$

Generally, the taper ratio (λ) value varies between zero and one.

$$0 \leq \lambda \leq 1 \qquad 2.2$$

Planforms' geometries Tapers are divided into three basic groups, as shown in Figure 2.2: rectangular, trapezoidal, and delta geometry. The rectangular wing configuration planform is inefficient due to its weak aerodynamic response. While it has certain advantages, such as low

cost and ease of manufacture, it also has a number of drawbacks. The rectangular wing design has a small downwash angle at the root and a large downwash angle in front. As a result, the attack angle at the tip is more likely to stall later than at the root[20,21].

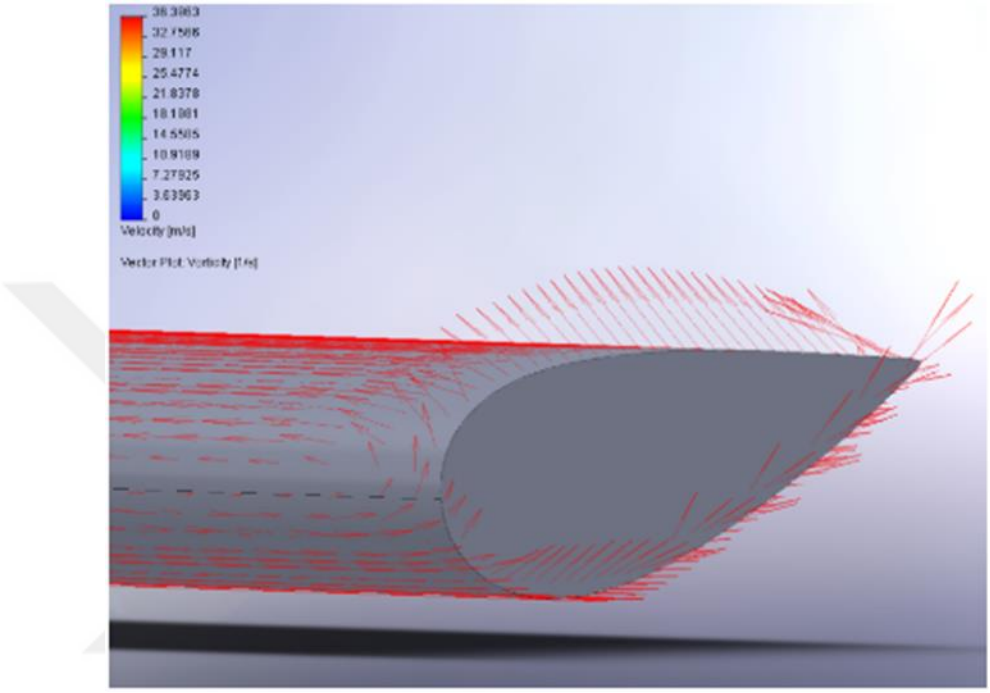

Figure 2.2: Wing Tip Configurations Configuration [21].

The effect of wing configuration taper can be summarized as follows[22,23]:

a) Wing configuration lift is supplied by variations in the distribution of wing configuration taper. This might be considered a taper advantage. As a consequence, the taper ratio was calculated based on the lift distribution parameters. The taper is expected to benefit this method.
b) The wing configuration taper raises the manufacturing cost of the wing.
c) One of the taper requirements is weight reduction. The taper will lessen the bending force at the wing configuration root due to the gravity of each wing configuration center's fuselage.
d) The mass moment of inertia of the wing arrangement about the x-axis (longitudinal axis) will be reduced. The aircraft's lateral control will improve as a result. The optimal taper in this circumstance is a delta wing configuration.

e) The taper will increase the aircraft's static lateral storability since it generally gives a sweep angle (either on the leading edge or on quarter chord line).

The taper ration can generate discrepancies in aircraft specifications due to its mixed influence.

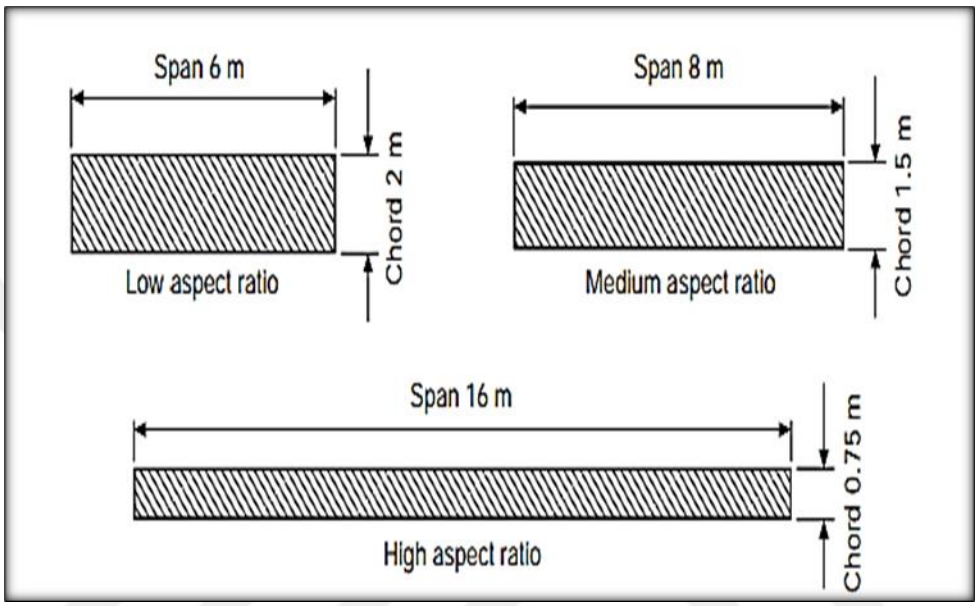

Figure 2.3: Observe the Aspect Ratios [24].

The ratio of span to chord is known as the aspect ratio. It depicts how long and thin the wing structure appears from above or below. You can pick from three different aspect ratios:

a) A stubby and short wing shape is indicated by a low aspect ratio. The structure is more efficient, and there is a higher instantaneous roll rate. They are more likely to be used by high-speed and fighter aircraft.

b) Wings with a moderate aspect ratio are the most typical.

c) High aspect ratio: This wing arrangement, which has a long and thin wing configuration with less produced drag and is more aerodynamically efficient, is used by high-performance sailplanes and high-altitude subsonic air.

The rearward slope of a wing arrangement is shown by the sweepback component in wing configuration plan form. A moderate degree of sweep can be used to adjust the center of lift when the wing design cannot be put in the best position for any reason, such as a pilot's vision from the cockpit. There are numerous different types of sweeps, as shown in Figure 2.4.

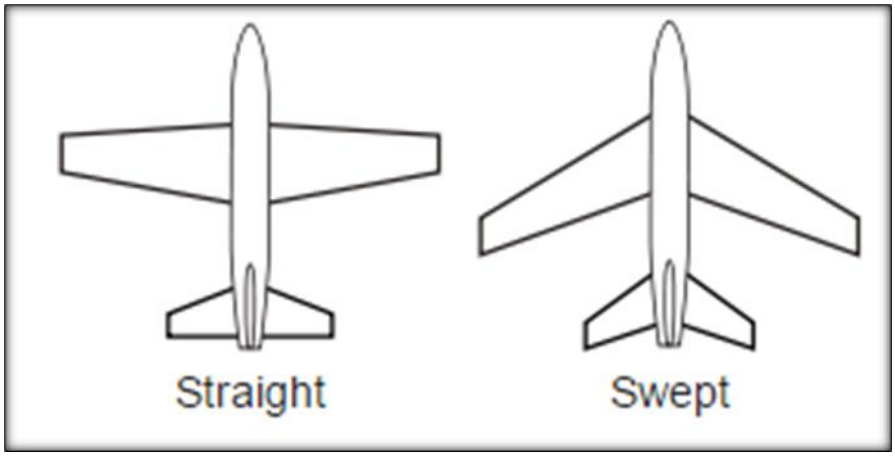

Figure 2.4: Traditional Types of Sweepbacks (www.Wikipedia.com).

The Straight type runs parallel to the flight path and is typically utilized in low-speed designs. During sweepback, the wing design sweeps rearward from the root to the tip, providing aerodynamic stability [16].

2.2 BACKGROUND OF AEROFOILS

A foil is a solid object that is placed at a proper angle into a moving stream to create lift force higher than drag. On the other side, the airfoil is the wing arrangement geometry through which the fluid passes to provide an aerodynamic effect. As the air flow rises, the static pressure decreases. Because air must travel a greater distance over the surface, it gains more velocity and loses more static pressure. Figure 2.5 shows the basic symmetric airfoil and the camber line, where t is the maximum thickness and c is the chord, as well as the cambered airfoil shape. These fundamental airfoil geometry features include trailing edge angle, leading radius, thickness ratio (t/c), and maximum thickening location y = yt(x). Leading edge slope, chord, maximum camber line displacement from chord location, and other factors are included in the camber line geometry y=yc(x). A fundamental symmetric camber line and an airfoil make up the cambered airfoil [25,26].

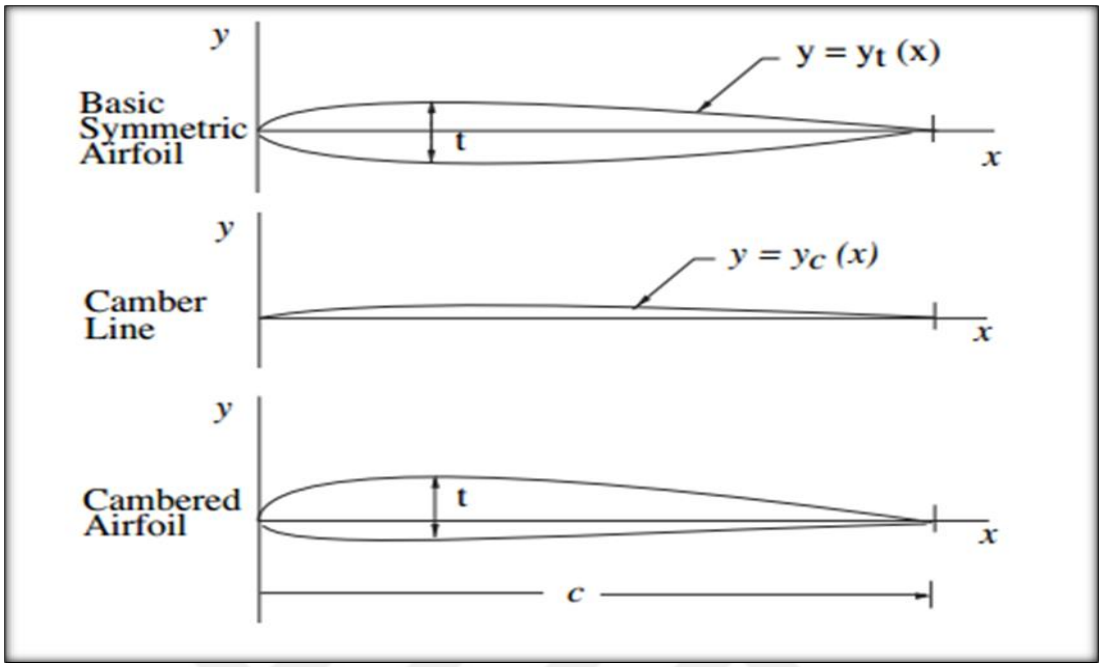

Figure 2.5: Airfoil Geometric Characteristic [25].

An airfoil's chord is an imaginary straight line that connects the trailing and leading edges. The chord length is the straight line that connects the leading edge of a chord to the following edge of the same chord. It is at this moment that the chord intersects with the leading edge. Figure 2.6 illustrates how the angle between the chord of an airfoil and the direction of airflow is calculated.

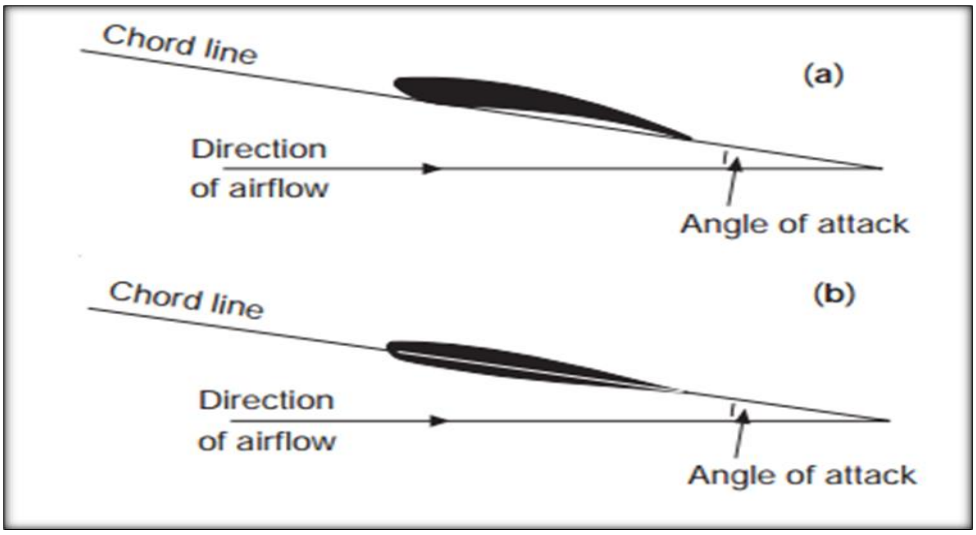

Figure 2.6: Chord Line and AOA, (a) Airfoil with Concave under Surface, (b) Airfoil with Convex under Surface [24].

The highest lift coefficient is created at the crucial angle of attack. The "stall angle of attack" refers to this angle. The angle of attack affects the drag and lift coefficients. The lift coefficients grow in proportion to the attack angle. As the angle of attack is increased, the lift coefficient rises until it reaches the stall angle value, the maximum angle value, after which it decreases. Airflow separation from the wing structure's top surface becomes more apparent with increasing fixed-wing attack angle, which slows lift coefficient expansion. At a 0-degree angle of attack, a symmetrical wing shape produces no lift. wing configuration geometry, including airfoil section and wing configuration planform, affects the lift curve. Curved wings have lower, flatter curvature, and a larger critical angle than straight wings [27].

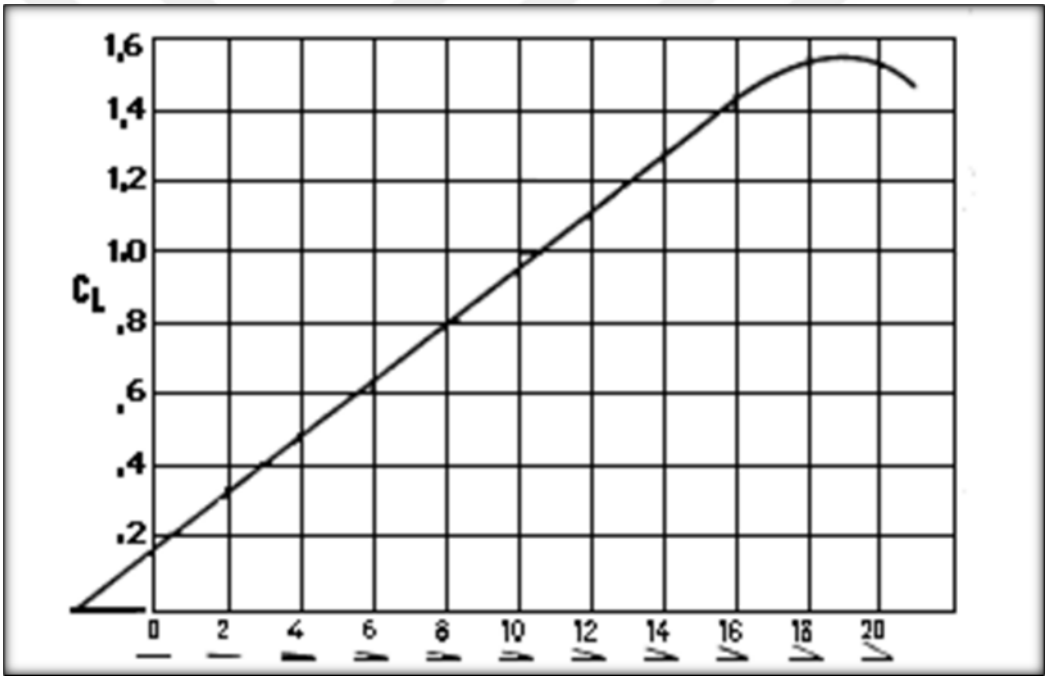

Figure 2.7: Lift Coefficient Curve [27].

The air pressure on the top surface decreases while the air pressure on the lower surfaces increases as a result of pressure fluctuations in the airfoil. A lift force will be generated as a consequence of the higher air pressure on the bottom of the vessel, as illustrated in Figure 2.8.

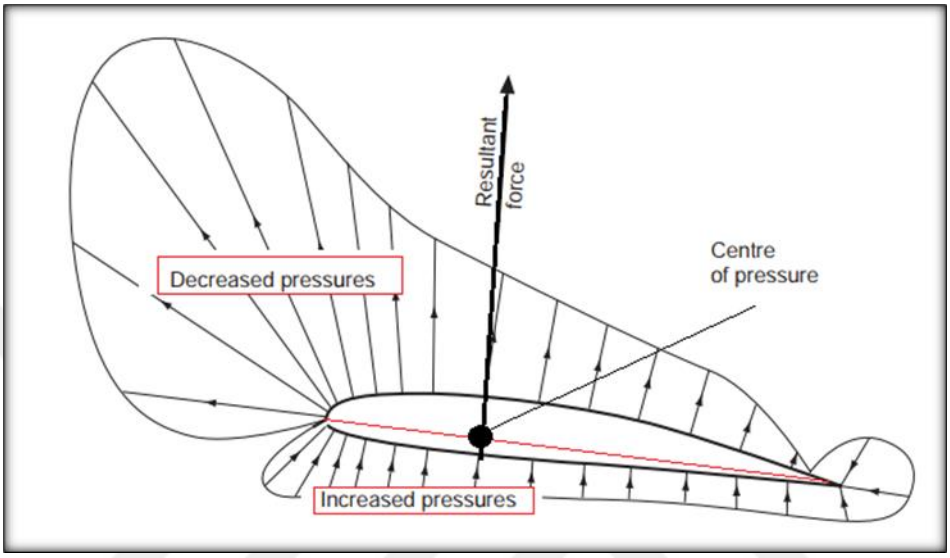

Figure 2.8: Pressure Distribution over an Aerofoil [24].

The current review focuses on the behavior of airfoils in airflow over a wing configuration. The following part will go through the principles of aerodynamics so that you can distinguish the different airfoil specs.

2.3 BACKGROUND OF AERODYNAMIC

Aerodynamic refers to how air flows around an object. As a result, the aerodynamic laws provide the basis of airplane flying. The study of the loads imposed by the flow of air over an airplane is commonly referred to as aerodynamics. As shown in Figure 2.9, these loads may be classified into six categories: three forces (side directions, lift, and drag forces), and three moments (Yaw Moment, Roll Moment, and Pitch Moment). To find the optimal loads in aircraft design, we need a thorough grasp of the aerodynamic principles that affect fuel consumption, airplane stability, control, and other flying challenges. This thesis will concentrate on the wing configuration design, which is the most significant part of the airplane. The wing configuration role is used to generate lift force, which is defined by Newton's third law and the pressure differential. The air

pressure on the lower surface of the wing configuration is greater than the air pressure on the upper surface, resulting in a pressure differential [28,29].

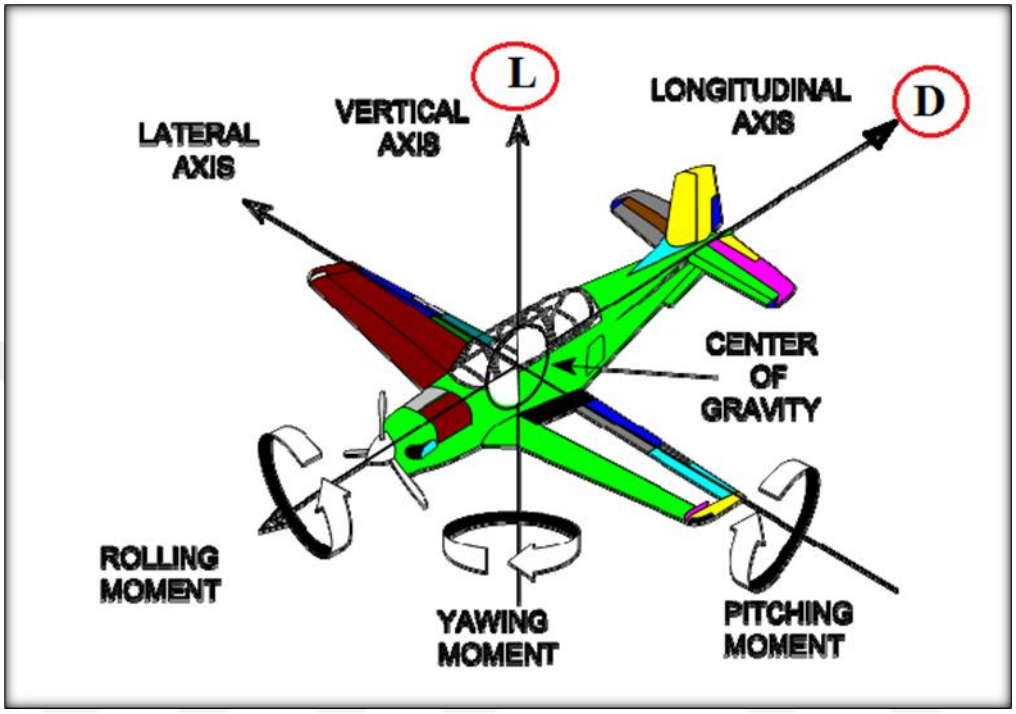

Figure 2.9: Aerodynamic Forces [30].

A force can be exerted upwards due to the pressure differential. While Newton's third law is concerned with wing configurations that push air toward the ground based on the movement power of airplane engines, the air pushes the wing configuration upwards with equal force. Mass, momentum, and energy conservation laws also apply. The present study will provide data on the forces that airflow conditions have on the body. These forces are created by the interaction of friction and pressure. For calculating the aerodynamic force acting on a wing form, the relationship between velocity and pressure is critical. The forces examined are part of the wing configuration impact; the drag is the other component. A drag force is applied to all bodies in a real airflow. It's the force that creates resistance when air passes through the plane while it flies. This resistance is known as drag [3].

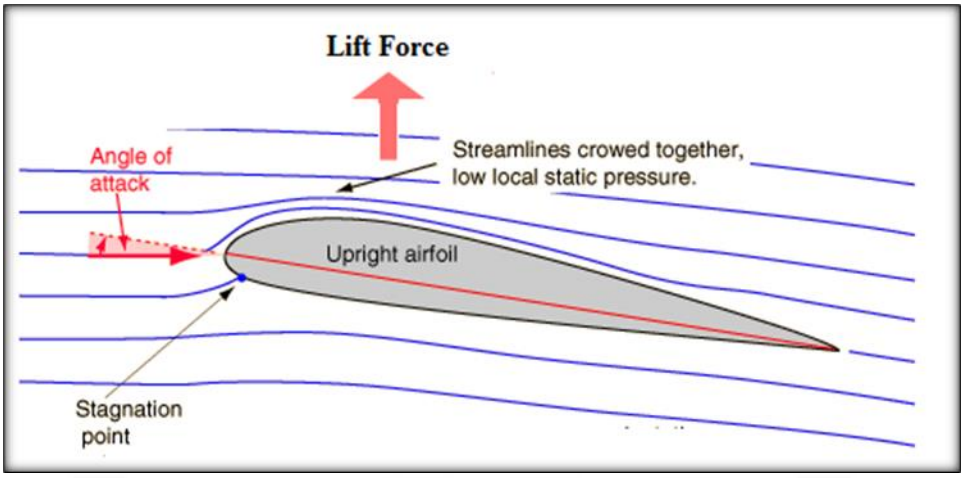

Figure 2.10: Airflow Forces [31].

The parallel force, often known as drag, is the first of two aerodynamic factors that cause these airfoil forces. The second aerodynamic effect is perpendicular force, sometimes known as the lift force, as seen in Figure 2.10. As seen in the picture, raising the angle of attack is obviously one of the most important features of the wing configuration impact. The chord angle of the wing section and the speed of the air stream combine to generate the main angle of attack. Airflow over the airfoil is almost smooth and laminar at very low angles of attack, with just a little turbulence impact at the trailing edge of the airfoil. Laminar flow and turbulence are separated at the separation point. As the angle of attack increases, the surface area of the wing structure facing the air stream increases. This increase in turbulent flow causes lift to rise, but it also causes laminar flow to separate from the airfoil, resulting in a rise in drag as the separation point advances closer to the leading edge. At a 15-degree angle of attack, the most lift is generated; however, this may be greater with unique airfoils. Disruption of the laminar flow occurs when the separation points creep up to the leading edge of the airfoil over 15 degrees. Lift is quickly degraded by turbulent air, while drag is greatly increased, which leads to stalling. As a bonus feature, this graphic illustrates the formula-based lift force impact on an air foil [32].

$$FL = \frac{C_L r v^2 AP}{2} \qquad 2.3$$

where:

C_L: the lift coefficient

v: is undistributed fluid velocity (m/sec.)

AP: is the area of airfoil as seen from the above.

The lift force influences a number of variables, the most significant of which is the lift coefficient. To simulate all of the complicated interactions between geometry, tilt, and specific flow conditions and lift, aerodynamicists use a lift coefficient, which is a non-dimensional variable. The lift coefficient is defined as the area multiplied by the ratio of the lift force to the dynamic pressure force. The Reynolds number, Mach number, surface roughness, air turbulence, attitude, and body shape all impact this value. The equation can be used to approximate the lift coefficient.

$$C_L = 2p * k * sin(a + b) \qquad 2.4$$

For small values of (b) and (c), the formula is valid, where (k) is a proportionality constant, (a) is angle of attack, and (b) is the negative of angle of attack based on zero lift (a). The angle of attack-related wing configuration geometry function is known as the lift coefficient. It is used as a reference to analyze the link between wing configuration design and angle of attack value, as illustrated in Figure 2.11. The drag force is generally proportional to the air stream velocity. The drag value is influenced by the size and form of the structure in relation to the wind stream [33].

Three sorts of effects contribute to the drag force. The profile drag is caused by the frictional resistance of the wing configuration as it passes through the air. The drag impact increases as air speed increases, causing swirls in the air flow.

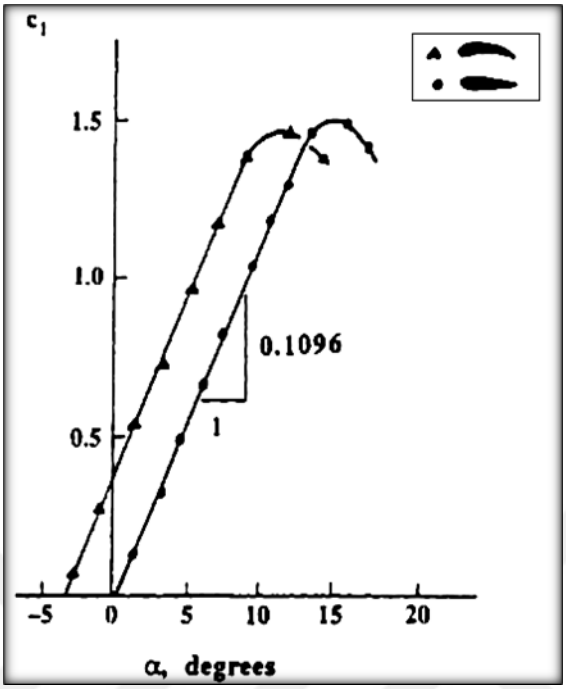

Figure 2.11: Correlation of Wing Configuration Design and Angle of Attack [33].

Form drag and skin friction make up profile drag. As seen in Figure 2.12, form drag is induced by the turbulent wake created by airflow separation from a structure's surface. [34,35].

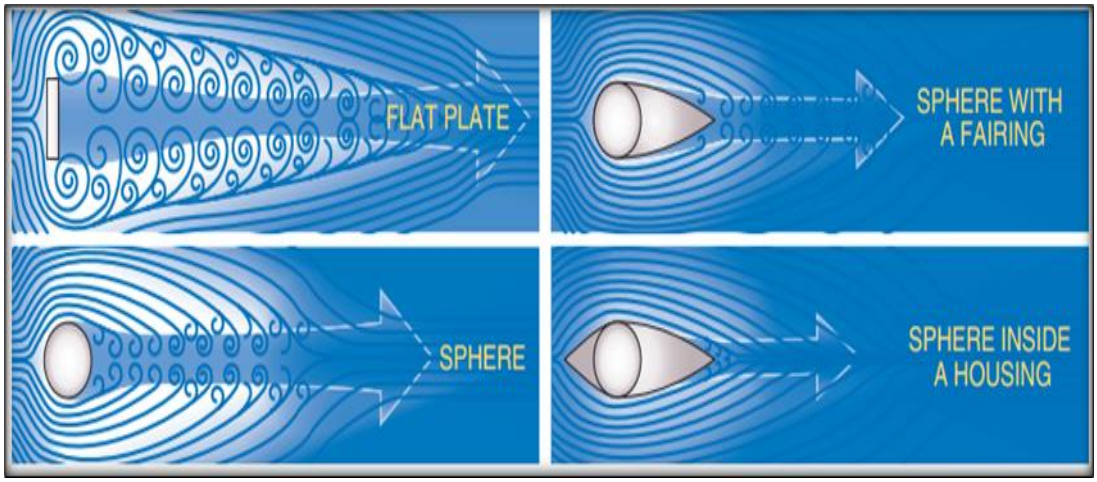

Figure 2.12: Airflow Surface Structure [34].

Induced drag is the second type of drag created by airflow circulation around the wing as it creates lift. Above the wing design, a low-pressure area links to a high-pressure area below it. Lift causes a spiral, or vortex, to form behind the wing configuration, as seen in Figure 2.13 [36].

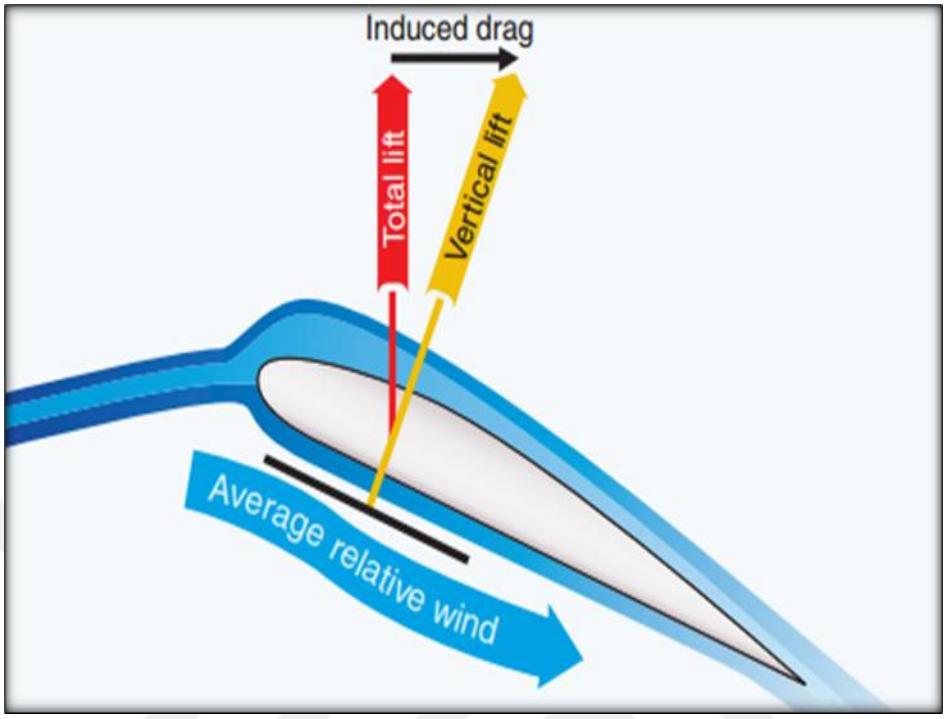

Figure 2.13: Induced Drag Profile [36].

The parasite is the third type of stumbling block. Traveling through the air in reaction to wind conditions is shown as parasite drag. This type of drag increases as airspeed rises. Whenever there is a loss of momentum in the airstream, parasitic drag increases. The chord angle of the wing section and the speed of the air stream combine to generate the main angle of attack. At very low inclinations, increasing airspeed causes site drag to grow rapidly, making it the primary source of drag. A four-fold increase in airspeed will result in a four-fold increase in parasitic drag. Figure 2.14 shows the total drag as the sum of the three drag forces.

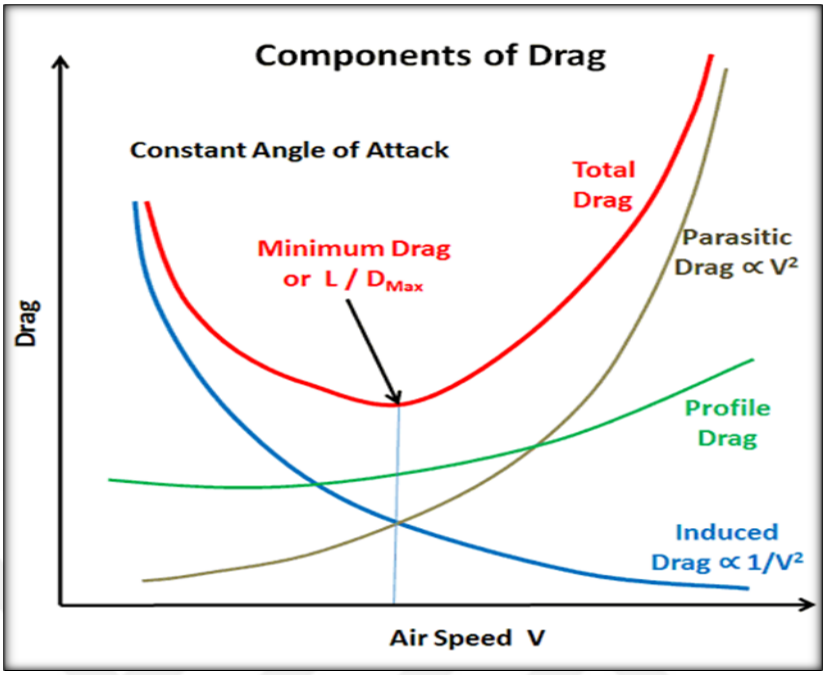

Figure 2.14: Drag Components [37].

A total drag curve is formed by combining all of the drag forces. Drag is reduced to its lowest level while flying at a low altitude. When L/DMAX is attained, the lift-to-drag ratio is at its peak. An airfoil's lift to drag ratio (L/D) is used to measure its performance. An airfoil with a high L/D ratio is more energy-efficient. The lift-to-drag ratio (L/D) is derived by dividing lift by drag. Drag has an impact on several factors, including lift force. The drag coefficient is also important.

A drag coefficient is a non-dimensional quantity [37]. The drag coefficient can be approximated by:

$$C_D = C_DQ + \frac{C_L2}{pAR} \qquad 2.5$$

C_DQ: infinite span drag coefficient

$$AR: b2/AP = AP/c2 \qquad 2.6$$

Finally, the Drag Coefficient translates changes in angle of attack into drag disparities. C_D is a collection of absolute numbers derived from wind tunnel measurements or mathematical computations, rather than a physical quantity. C_L and C_D, in addition to AoA, also rise as the angle of attack increases and are linked to lift force and drag.

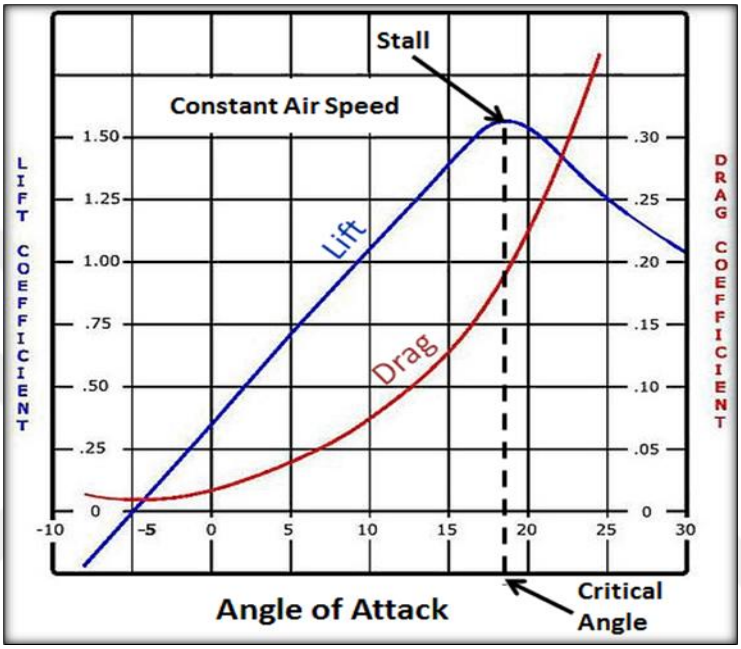

Figure 2.15: Critical Angle of Attack**.**

Once the lift starts to decline, the drag significantly increases. The Critical Angle of Attack (CAA) is a term for this position. All lift will be lost if the attack angle exceeds the Critical Angle of Attack, but drag continues to build, as shown in Figure 2.15. According to the proposed overview, the growth of flying aerodynamics requires more specific development skills.

3. METHODOLOGY

This chapter describes computational fluid dynamics (CFD) methods that may be used to examine the behavior of airfoils. Numerous numerical methods and computer algorithms are used in the process of evaluating and resolving air flow issues. Construct a computer model to examine the properties of airfoils in a simulated wing channel, and then assess the wing section impact by combining the lift force, lift coefficient, and drag coefficient with the angle of attack. CFD enables the modeling of the interaction between an airfoil and a range of effective factors and starting conditions. By using partial differential equations, the model will be reduced to a collection of control volumes. CFD Analyzer will be used by the solver to generate the conservation equations for mass, momentum, and energy. These equations will be used for the conservation of mass, momentum, and energy, respectively. In terms of the data and assumptions, as seen in Figure 3.1, this chapter employs the conventional methodological approach to supply all of the experimental data necessary for the project.

3.1 MODEL DEVELOPMENT

The model implementation technique will be presented in this section. The ANSYS FLUENT software which is use the finite element method for solving the problems [38,39]. which is based on the chosen model, is used to address CFD issues. The overall simulation technique employed in this inquiry is depicted in Figure 3.2. Based on the three-wing form design in this part, the researcher creates the processes for generating the simulation model. The symmetric type will be used as a baseline for analyzing the airfoil behavior of the other two kinds. The pre-processing stage comprises constructing to produce the mesh, followed by fixing the physical model, boundary conditions, initial conditions, and other necessary parameters in the model's step, then solving, and lastly the post-processing step.

In the post-processing stage, the experiments that may be employed to produce findings across the computational domain.

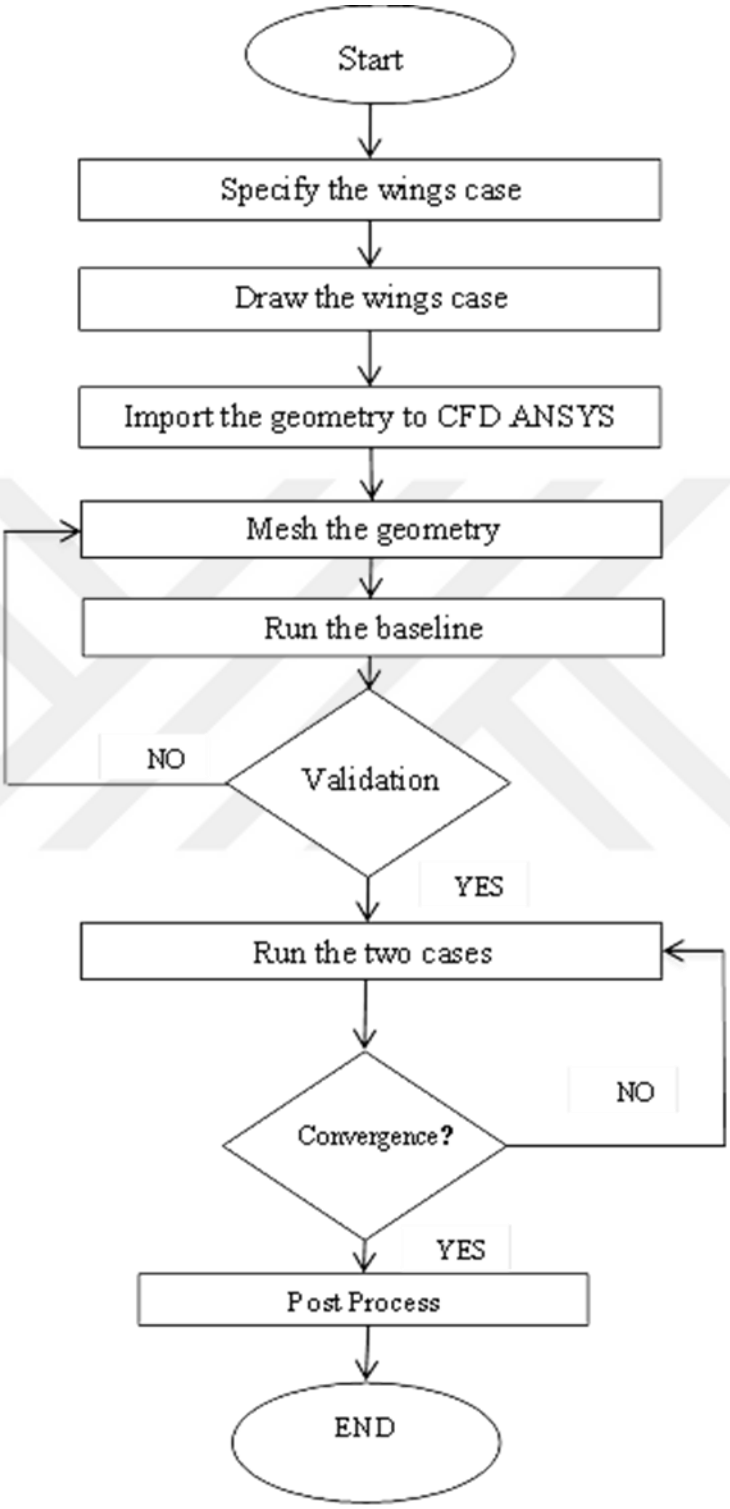

Figure 3.1: Flowchart of the Project.

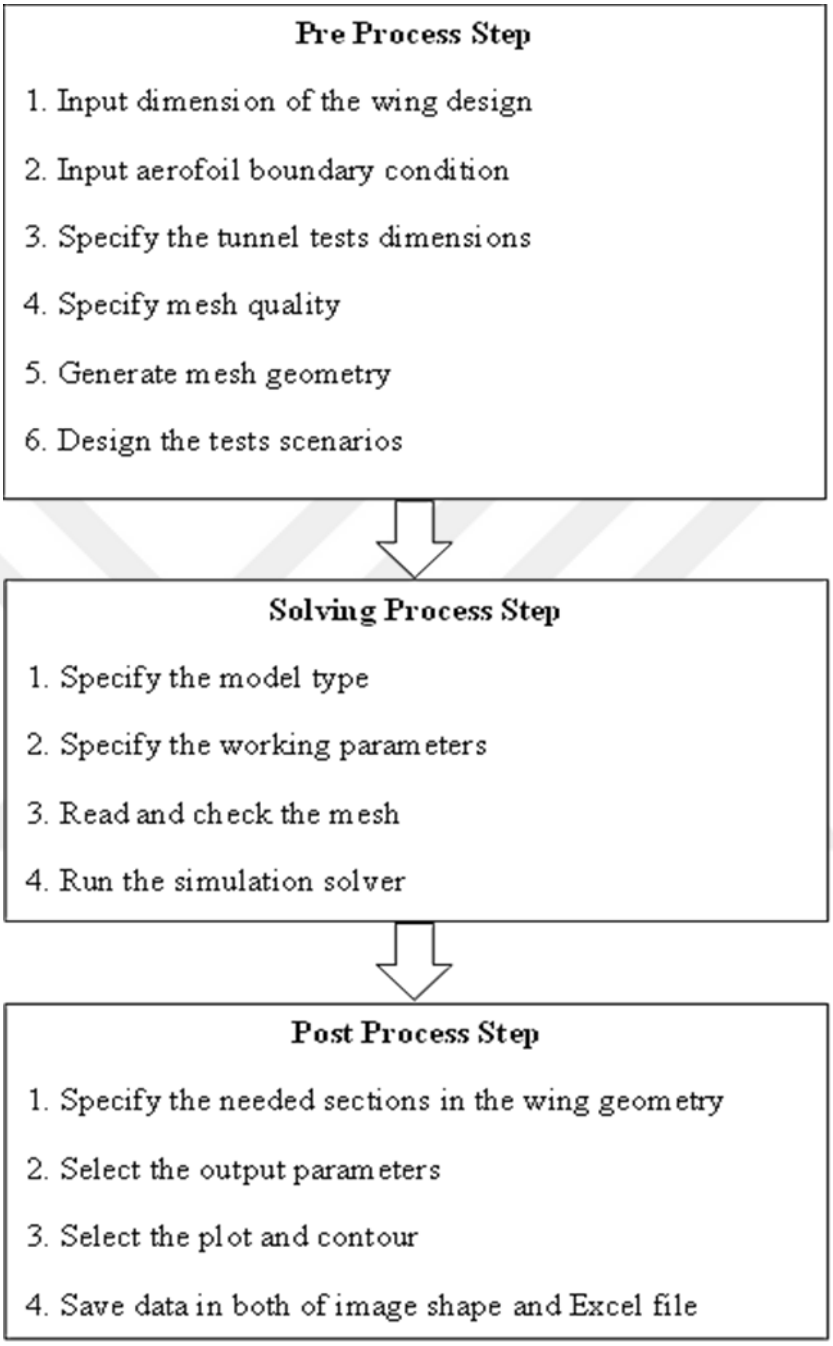

Figure 3.2: The CFD Modeling Sequence.

3.2 PRE-PROCESS STEP

By double-clicking the Fluent option in the Analysis Systems section of the Toolbox, fluid flow analysis systems may be generated in ANSYS. Figure 3.3 depicts this concept.

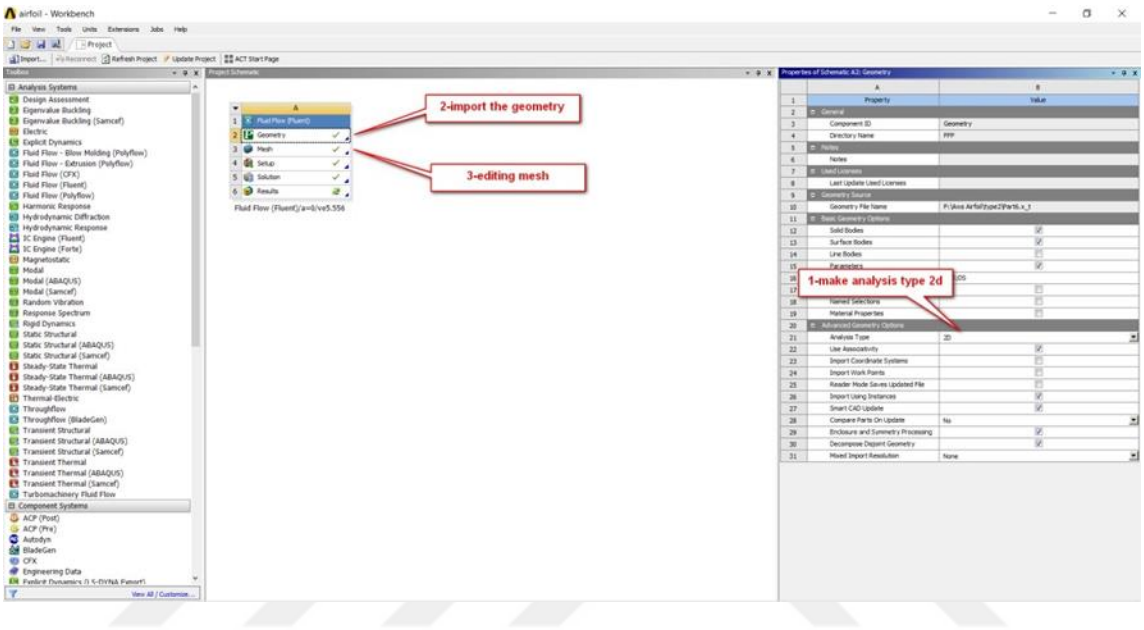

Figure 3.3: Fluid Flow (Fluent) Files.

The fluid flow analysis system consists of several cells, some of which are named geometry, others mesh, etc. Due to the fact that ANSYS Workbench is comprised of a range of data-integrated and native applications operating in a single, continuous project flow, individual cells within ANSYS Workbench are able to receive data from other cells and transmit data to other cells. Then, we will proceed to construct the geometry.

Step 1: Creating the Geometry

The first stage in creating the computational wing geometry is to complete this phase. This stage requires the standard wing form data set, which is freely available online. The dimensions will be supplied when the geometrical dimensions are uploaded to the SolidWorks [40,41]. These dimensions indicate the airfoil's boundary conditions, as seen in Figure 3.4. The wing form geometry comprises configuration conditions such as wing taper, wing length, and wing width, as shown in Figure 3.5. The effective parameters of the wing design impact include these data needs.

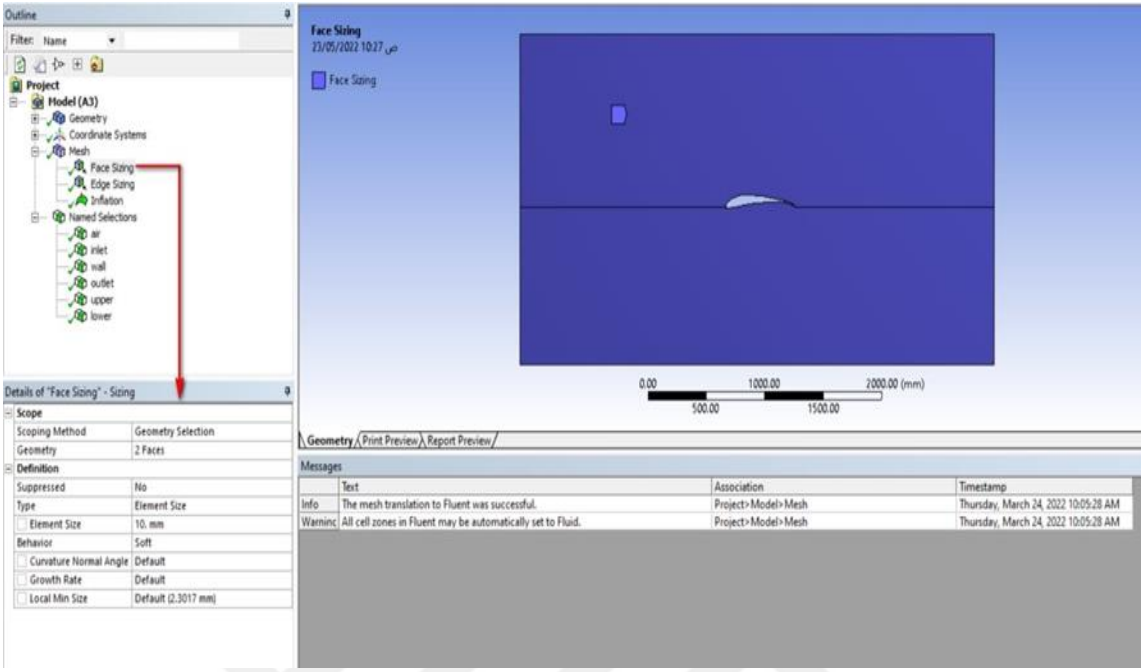

Figure 3.4: Setting of the Domain Size.

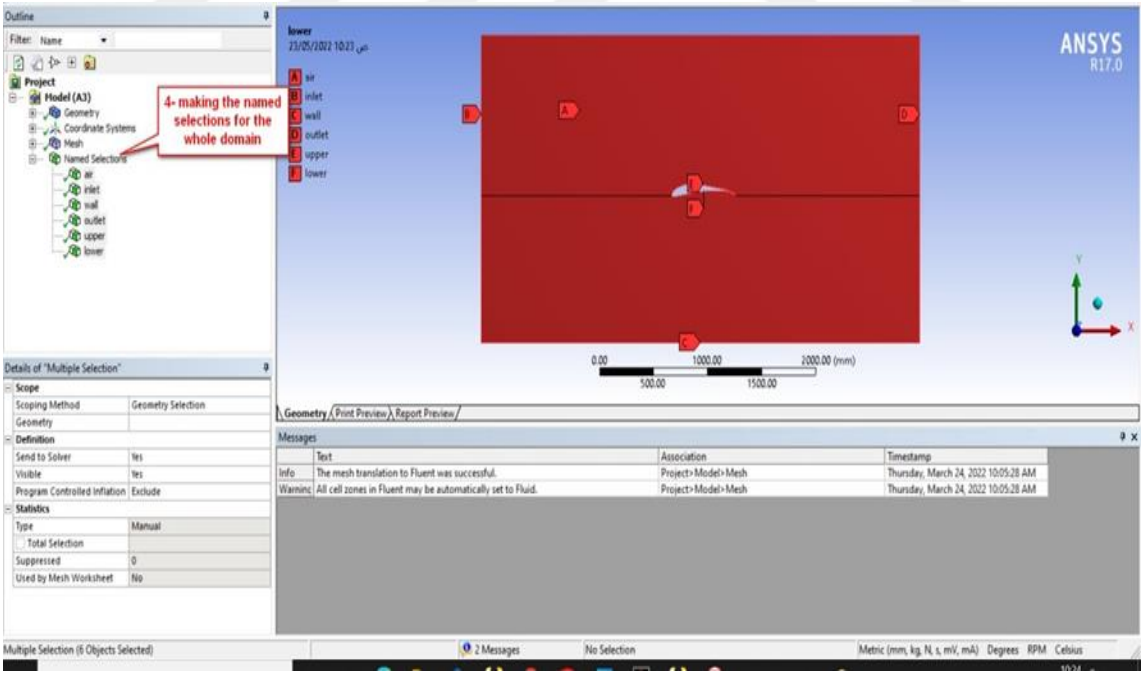

Figure 3.5: Selection of the Domain Name.

After preparing the 3D wing shape, the step of creating mesh will be the next.

Step 2: Meshing the Geometry

Meshing divides the form into an endless number of little finite elements. By meshing these elements, we may examine the behaviour of a variety of factors (such as pressure, velocity, and so on). The present method entails constructing a computational mesh that covers the full tunnel volume. This step, as shown in Figure 3.6, necessitates the use of the ANSYS Meshing program to generate a mesh for the CFD analysis. To make an object mesh, follow these steps:

a) To construct a mesh for the CFD study, choose the ANSYS Meshing program.

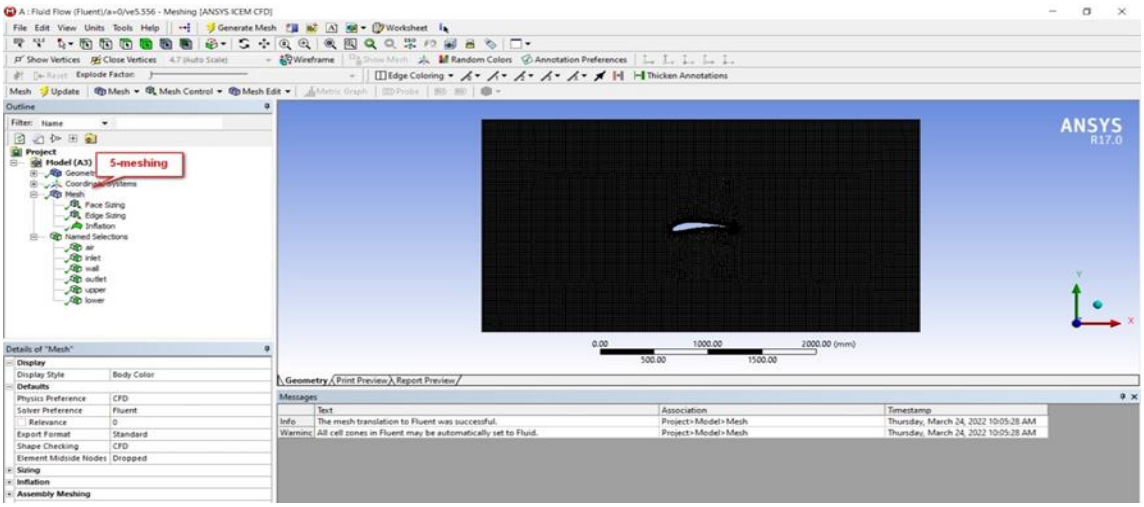

Figure 3.6: ANSYS Mesh Application.

b) As shown in Figure 3.7, provide the mesh quality control criteria to determine the optimal size and kind of mesh. These variables will influence the accuracy of the results.

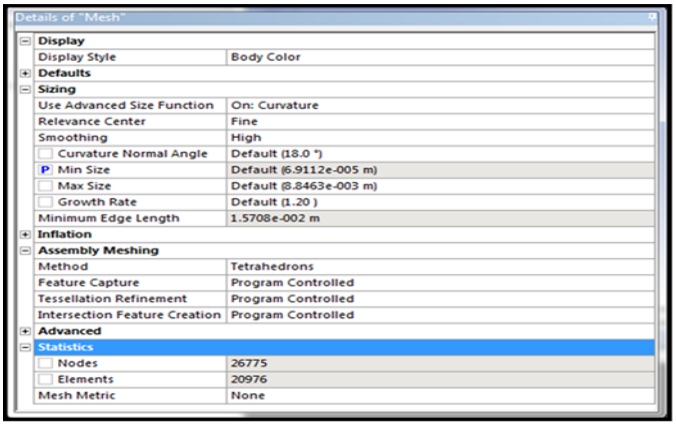

Figure 3.7: Mesh Quality Control Parameters.

c) The mesh metric will provide a bar graph to examine the mesh element quality in order to view advanced mesh data. As demonstrated in Figure 3.8, the bar graph will indicate the minimum and maximum element quality values.

Figure 3.8: infilation settings.

The best numerical mesh results summarized in Table 3.1:

Table 3.1: Best Numerical Mesh Results Values

Parameter	Value
Elements	7680969
Nodes	1658358

Step 3: CFD Simulation Set-Up

The best mesh results for selected geometry will transfer to the CFD analysis using the ANSYS Fluent. The procedure of this work is as in follows:

a) Start ANSYS Fluent

The Fluent Launcher allows starting up ANSYS Fluent based on the pre-processed geometry as shown in Figure 3.9.

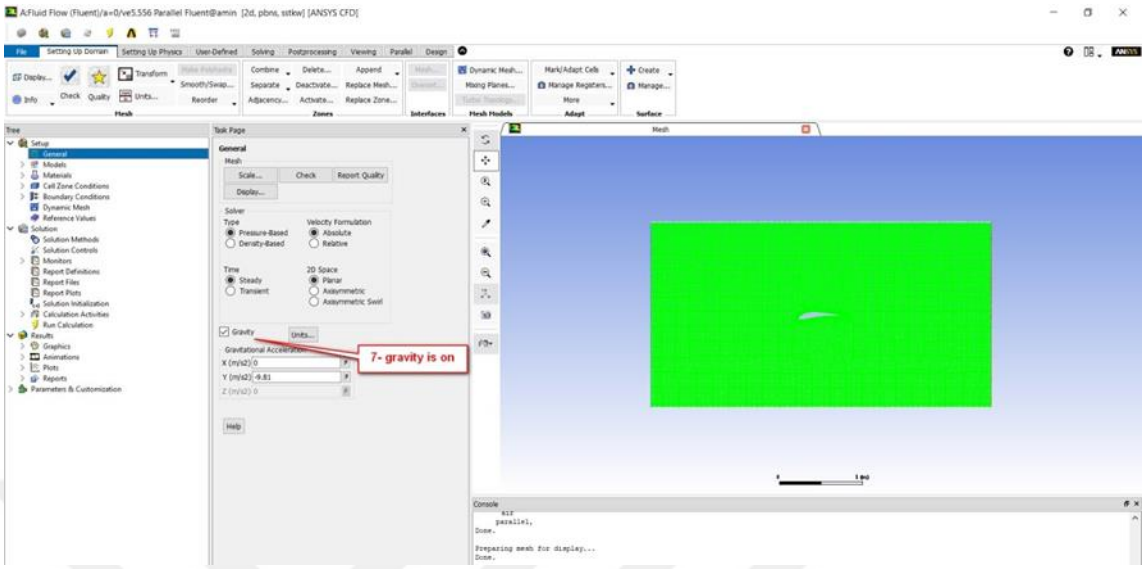

Figure 3.9: Fluent Launcher.

To solve the study scenarios, the general procedure will apply based on the meshed geometry conditions as in the sequence below:

A. Change the units for object dimensions. This step involves:
    a. Select length in the Quantities list.
    b. Select the millimetres in the Units list.
B. Check the mesh results.
C. Secify the air flow direction.

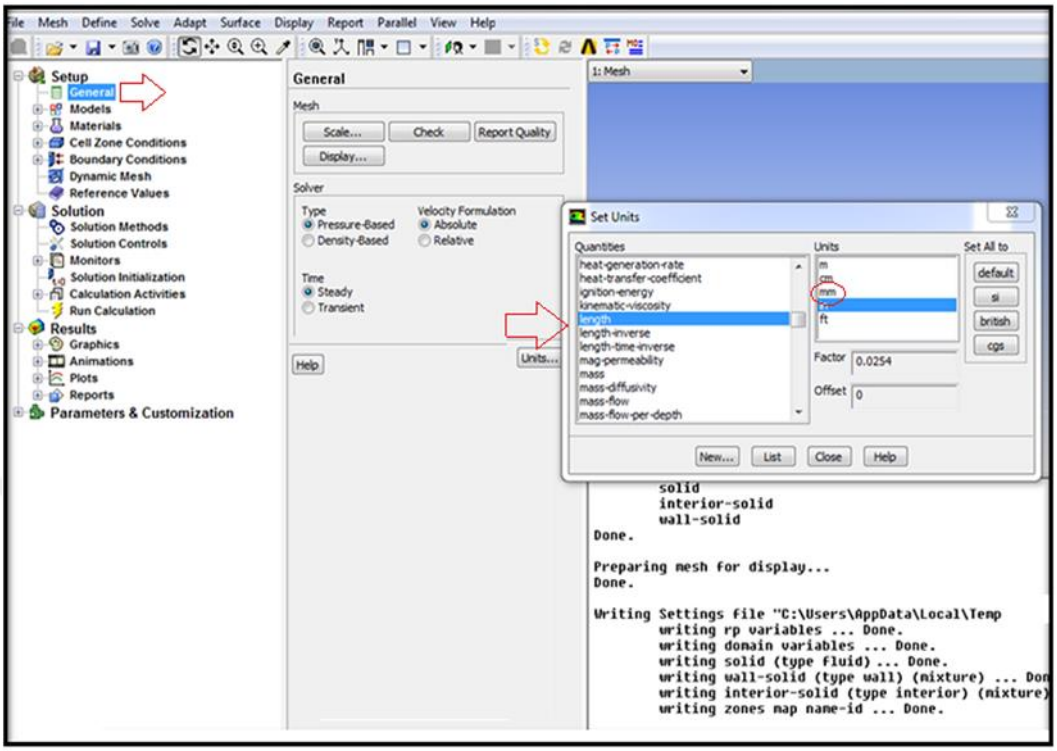

Figure 3.10: General CFD Settings.

Step 4: Setup the Model

The researcher will choose the model in this stage based on the prior investigations reported in chapter two. The aerofoil needs will be covered by the model, which will provide the necessary information depending on the working parameters of the specified kind of wing. The following is the sequence of the independent procedure:

a) Choose a model type from the Models Code list. The SST k–turbulence model, as introduced in chapter two, will be used in our case study.
b) Enable the k-turbulence model and select the optimal k-epsilon Model from the list in Figure 3.11.
c) Using the Create/Edit Materials dialog box, create the materials.

Step 5: Set up the boundary conditions

The 3D Reynolds Navier-Stokes equations for mass-averaged velocity, time-averaged pressure, and density are solved using the FLUENT program.

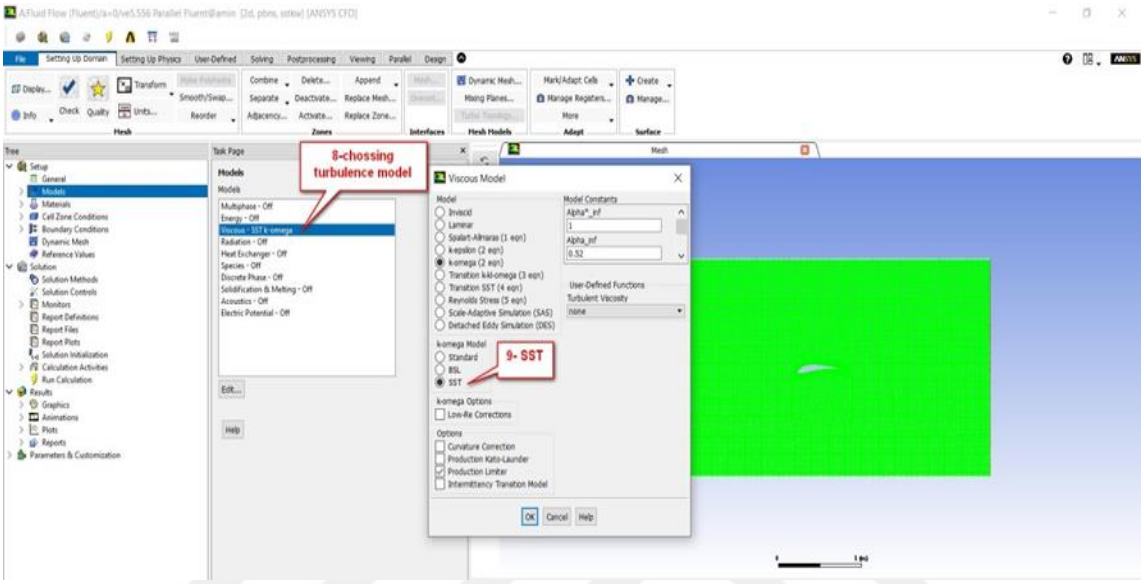

Figure 3.11: Models setup.

The software is a multi-dimensional Navier-Stokes fluid flow prediction system that is integrated and sophisticated. Because it combines a flexible, multi-block grid design, a graphical interface, and several advanced modelling tools, it's ideal for water flow simulation. The air velocity, as illustrated in Figure 3.12, is the key input representation for this investigation.

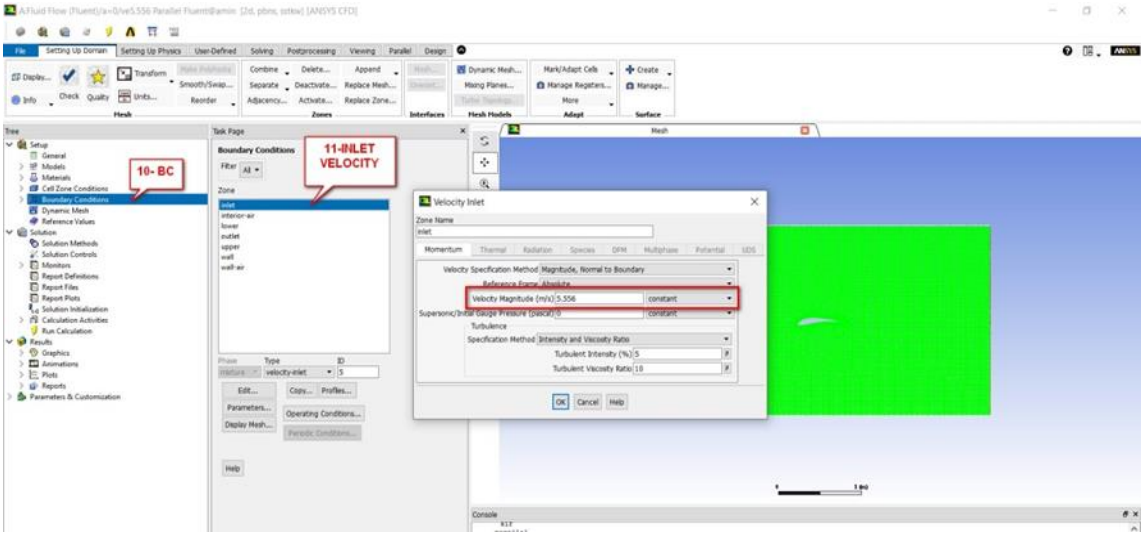

Figure 3.12: Set Up the Boundary Conditions.

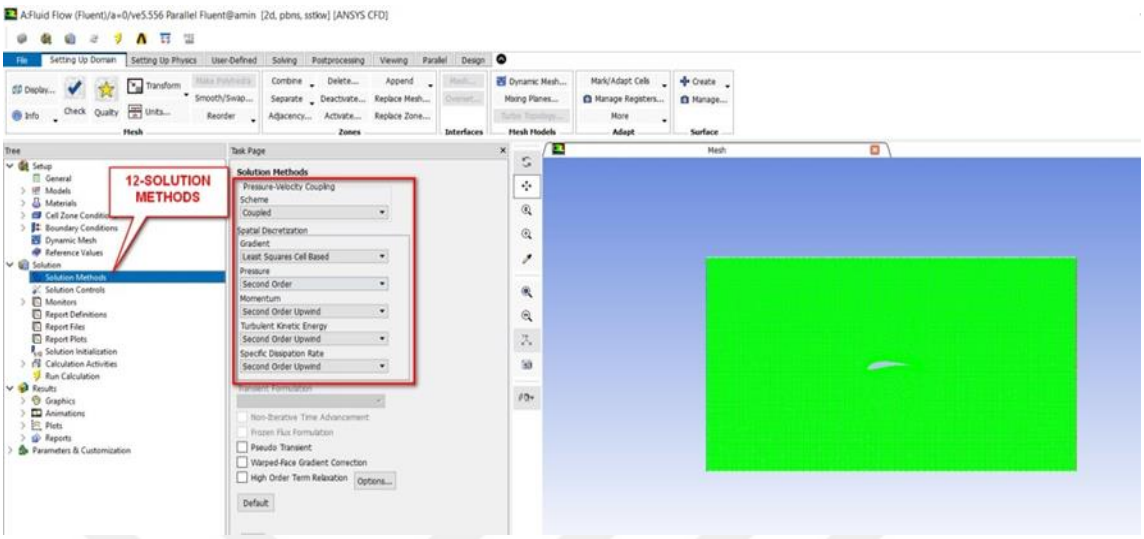

Figure 3.13: Specify the solution methods.

The boundary conditions of the system simulation will be controlled by the input representation. In this stage, the counties' simulation settings will be changed.

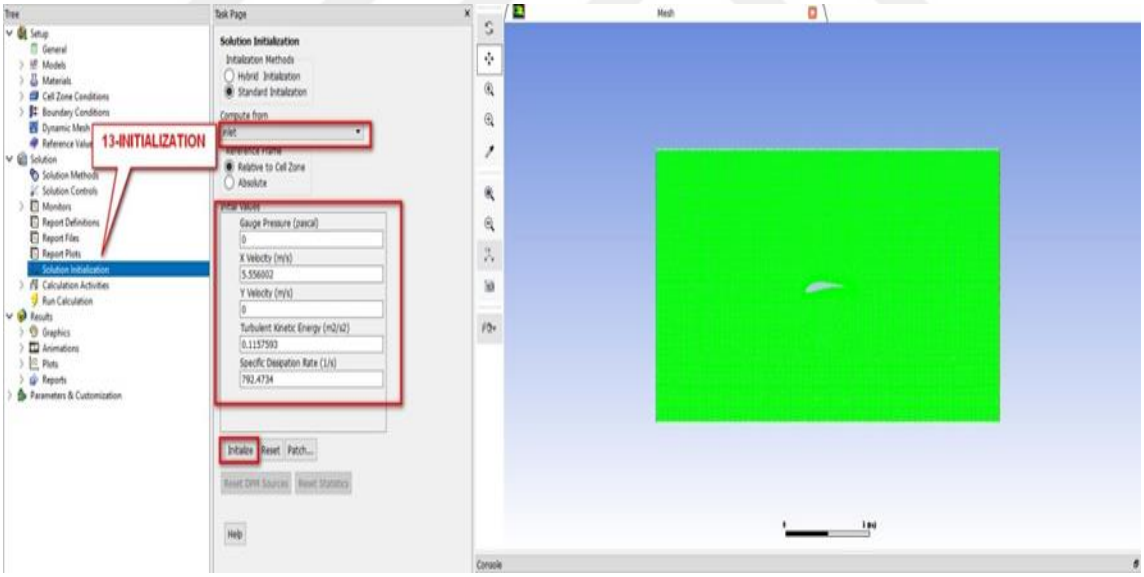

Figure 3.14: Specify the Initialization Process.

Step 6: Run the solution

Running the solver is a critical step in ANSYS. It's a valuable tool for explaining airfoil behaviour. The number of iterations and the date of the working variables are essential in this stage.

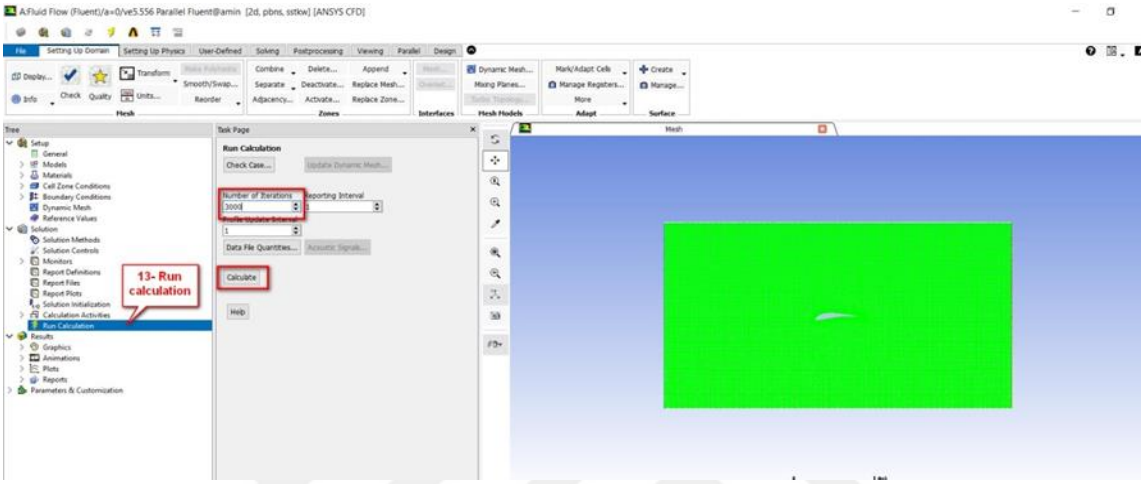

Figure 3.15: Run the Solution Process.

The FLUENT fluid flow solver may be used to handle incompressible, compressible, steady state, transient, laminar, and turbulent single-phase flow problems in complex geometries. Consequently, it is feasible that system simulations may be able to identify a few specifics of how distinct airfoil deviations may be caused by different changes in conditions.

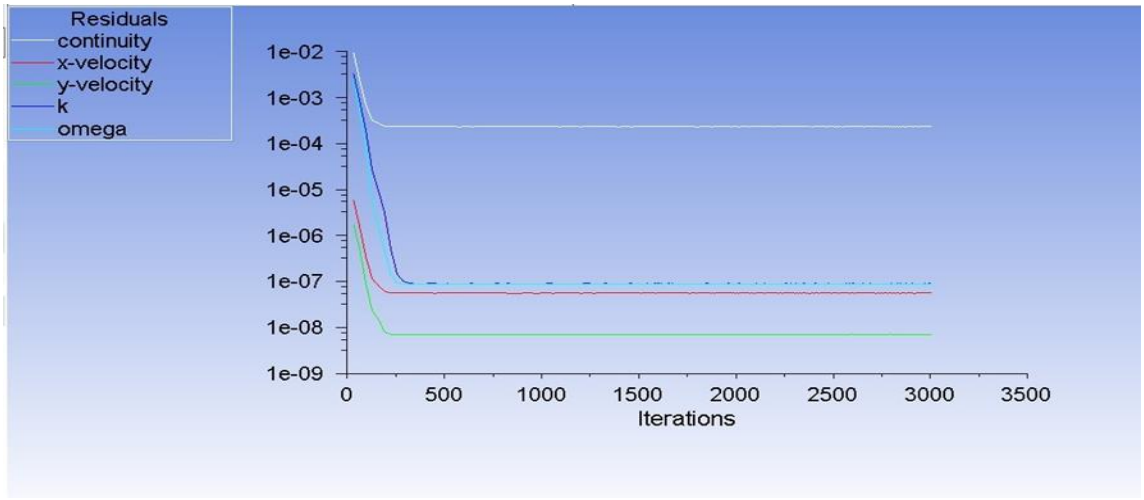

Figure 3.16: Calculation Processes.

4. RESULTS AND DISCUSSION

Different wing design analyses have looked at the aerodynamic characteristic's changes in the airfoil effects. To determine the air behavior moving on the wing surface that provides the classic lift force and drag responses, it usually involves knowing the wing particular shape design. The current study creates a series of simulation experiments using various airfoils and velocities at various angles of attack. The chosen airfoils are from the S1223 Airfoil (s1223-il) and S1223 RTL AIRFOIL (s1223rtl-il) families, which represent two common applications in this sector.

The simulation was performed using the ANSYS CFD Fluent program, and the results were validated using the baseline. This phase is required to assess the CFD method's correctness. The validation test is a technique for reducing and quantifying modeling mistakes and ensuring that the CFD model being solved is accurate. The analytical research must be completed before the validation in order to analyze the effect of changing any single parameter in the simulation. Analytical assessments of node number, grid types, and turbulence models were undertaken in this work.

The findings of the CFD simulation meet the study's goal and give a brief discussion based on the S1223 airfoil and S1223 RTL. The first section presents the ANSYS findings and plots their special numerical results, while the second section examines the differences between the two types of airfoils currently available.

The NACA 0009 airfoil was employed as a case study for this research's validation. The multi-angle of attack has been utilized to detect pressure and velocity variations on the aircraft airfoil. All of the findings were compared to earlier air speed investigations. The data from Sandia National Laboratories (SNL) and Sheldahl and Klimas from 1981 were used in independent research for comparison. To characterize the variations in flow behavior in the airfoil domain, the SST k-w turbulent model is employed. Figures 4.1–4.8 depict a collection of velocity and pressure profiles depending on different angles of attack.

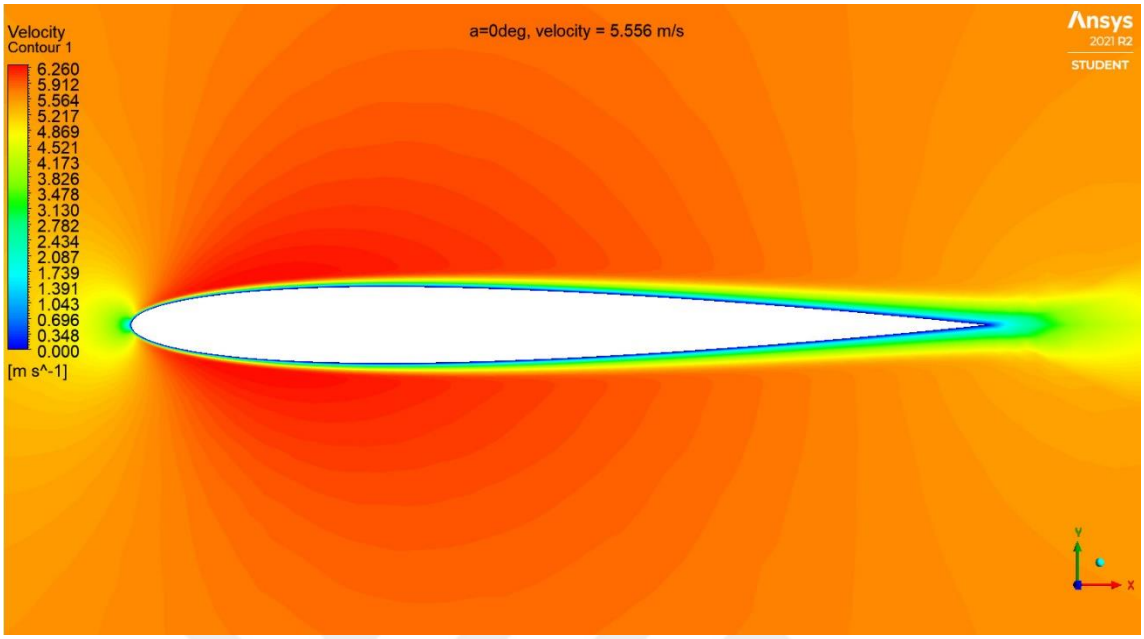

Figure 4.1: velocity Profile of NACA 0009 v=5.5m/s.

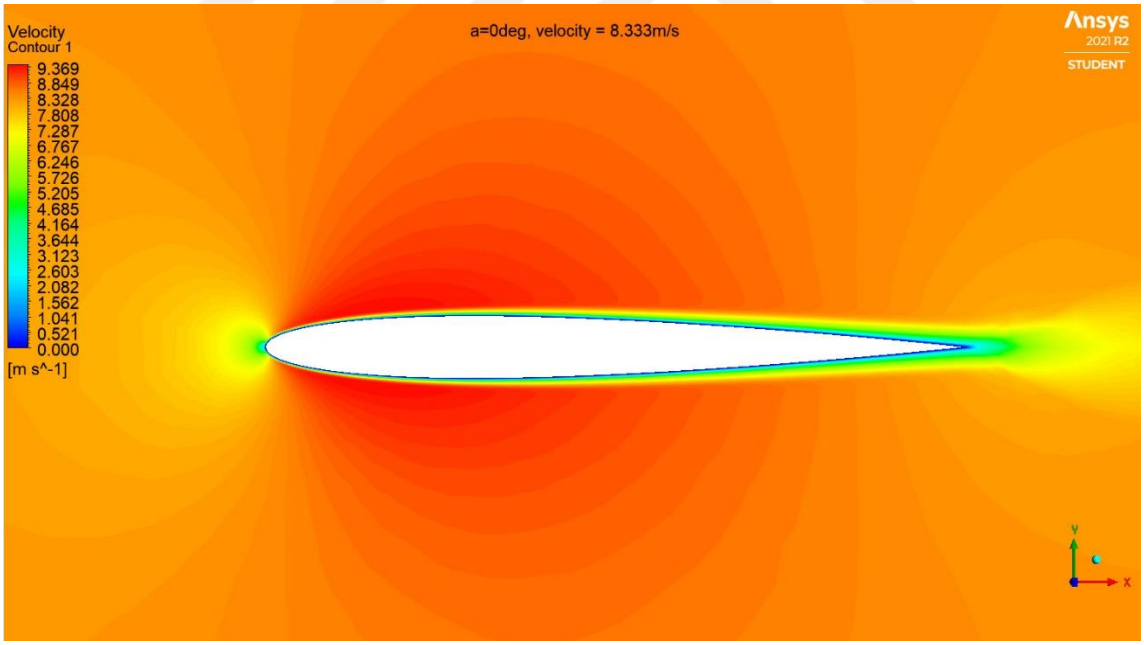

Figure 4.2: Velocity Profile of NACA 0009 v=8.3m/s.

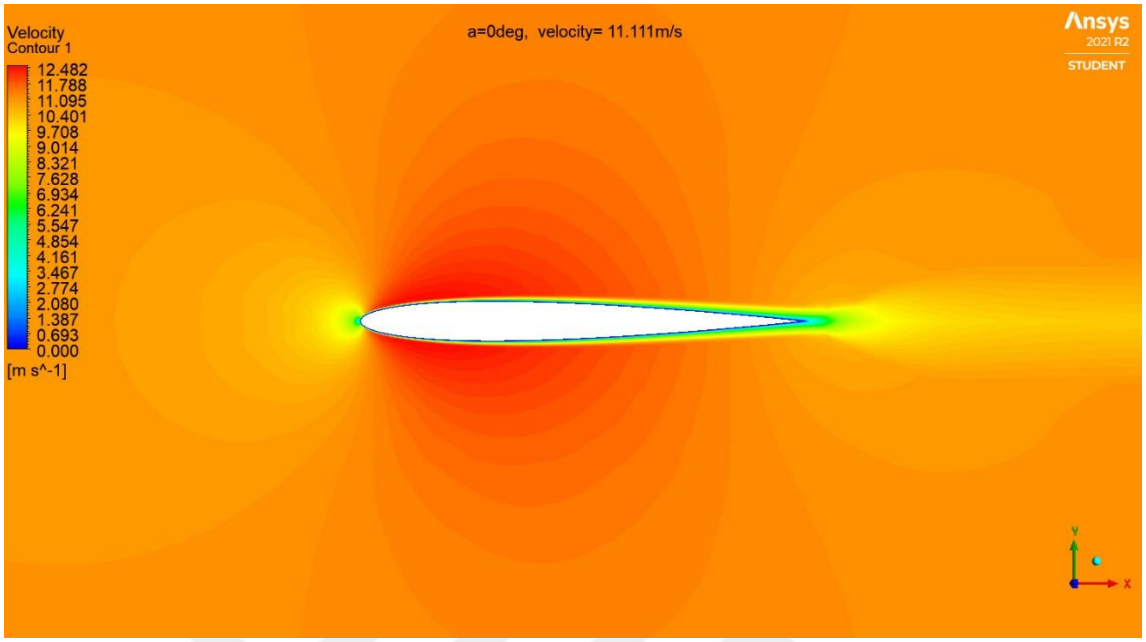

Figure 4.3: Velocity Profile of NACA 0009 v=11.11m/s.

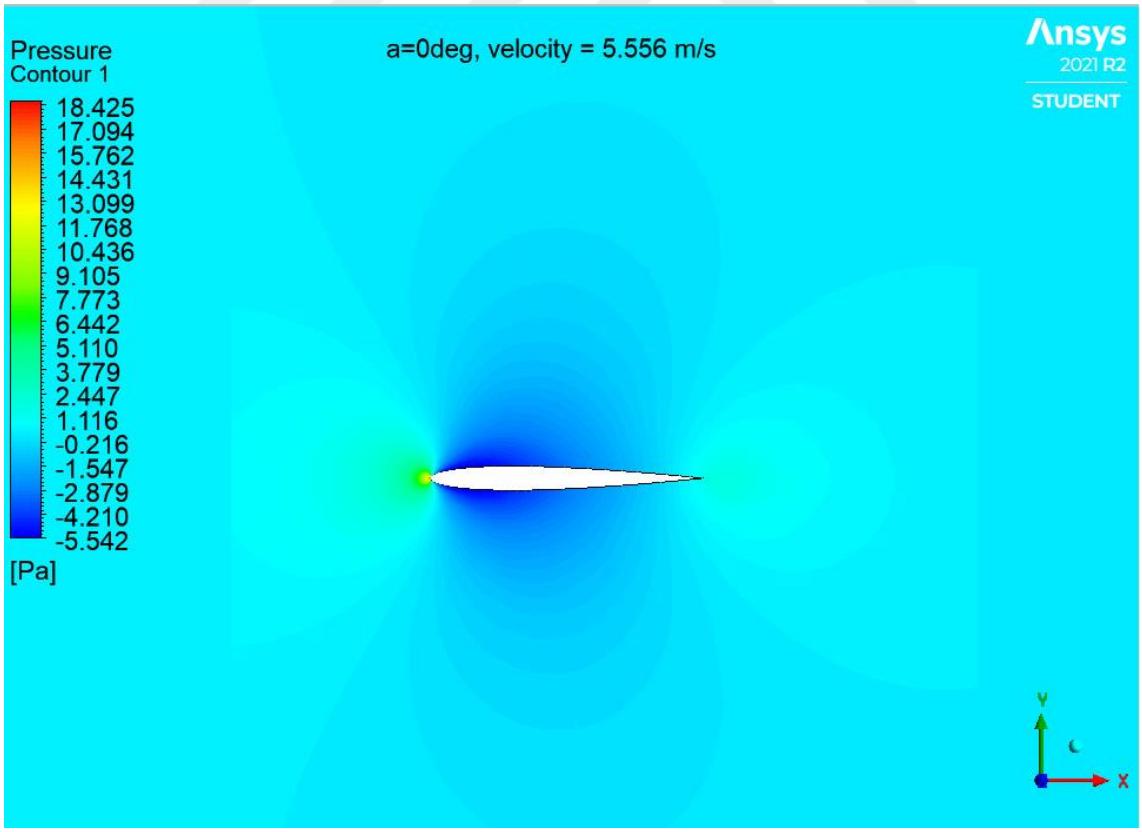

Figure 4.4: Pressure Profile of NACA 0009 v=5.5m/s.

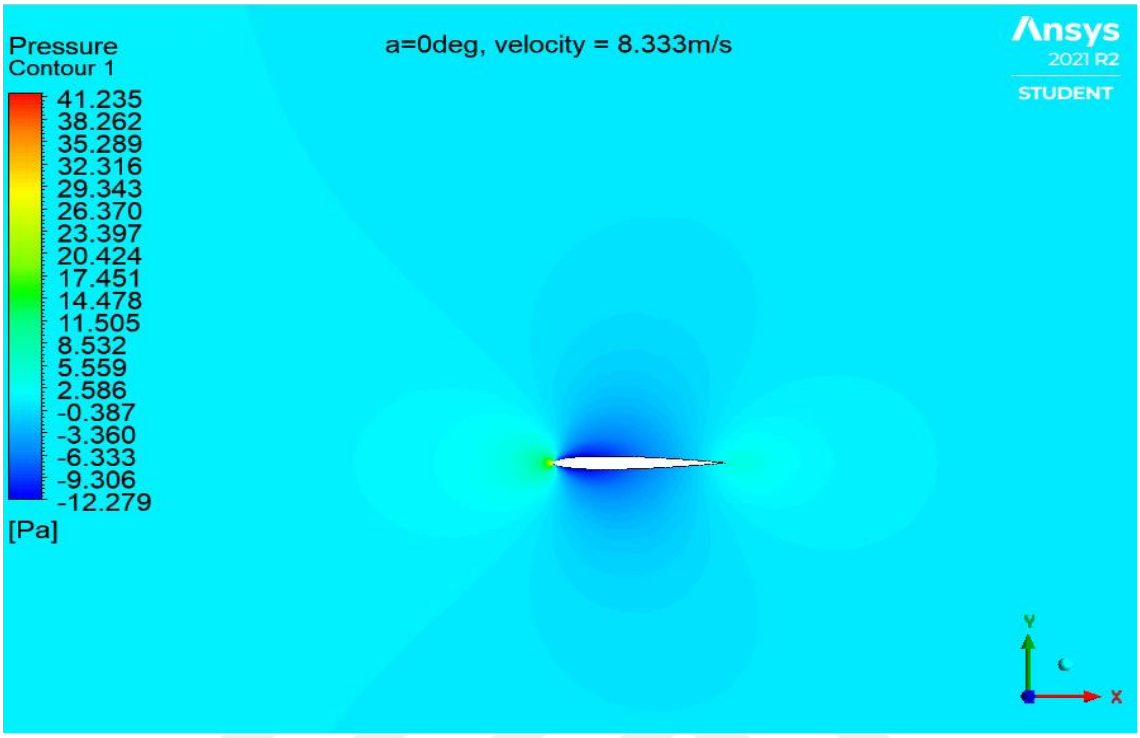

Figure 4.5: Pressure Profile of NACA 0009 v=8.3 m/s.

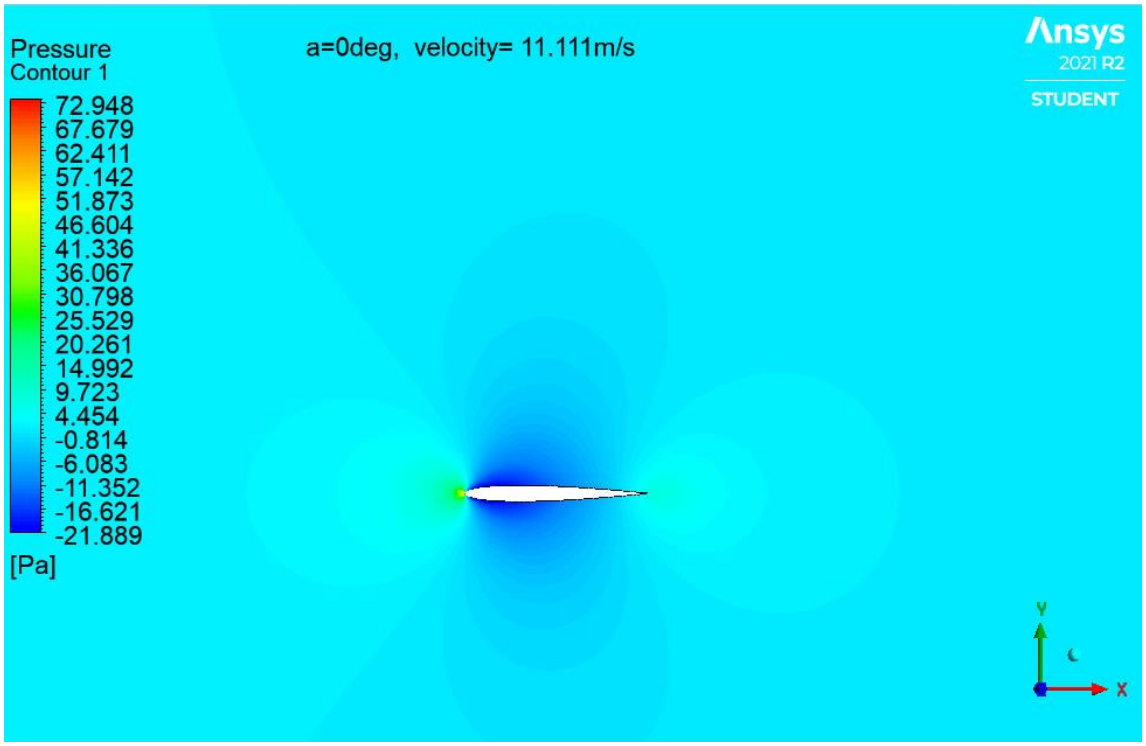

Figure 4.6: Pressure Profile of NACA 0009 v=11.11 m/s.

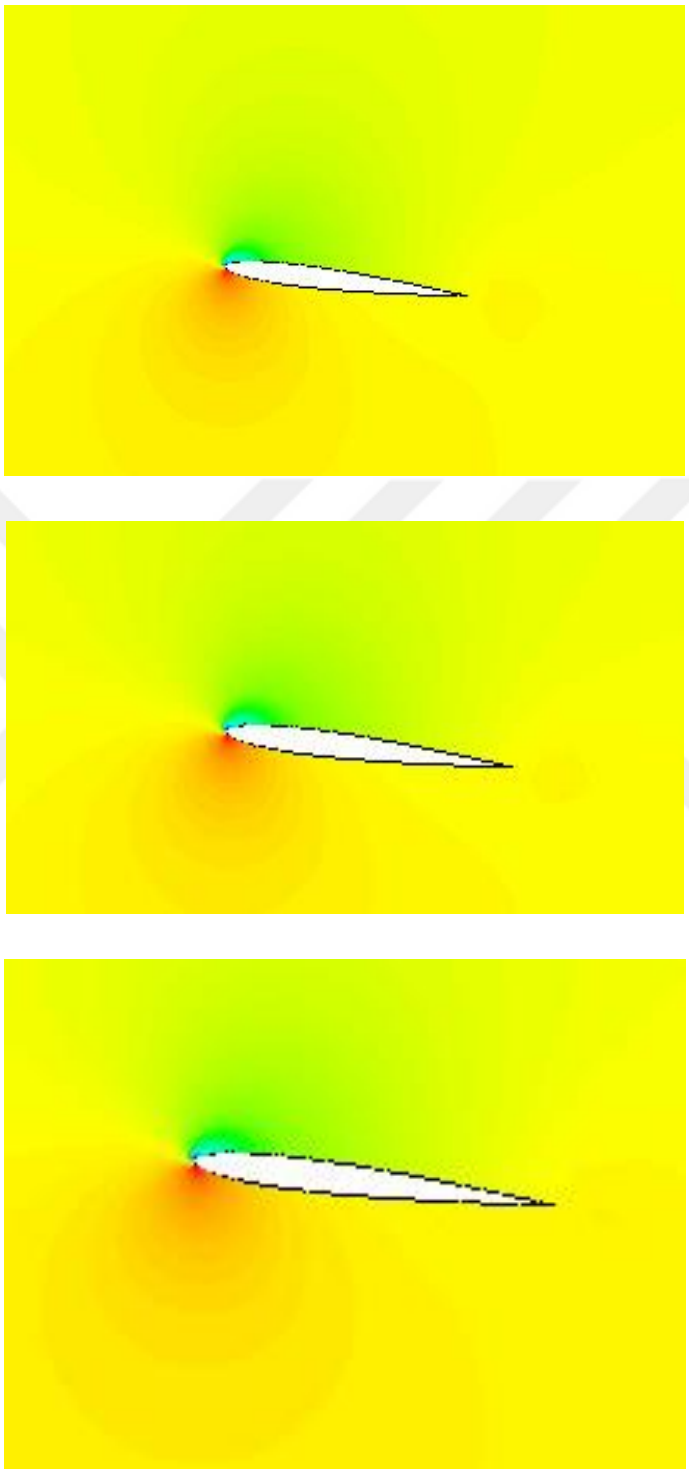

Figure 4.7: Pressure Profile of NACA 0009 at 70 with Different Velocities.

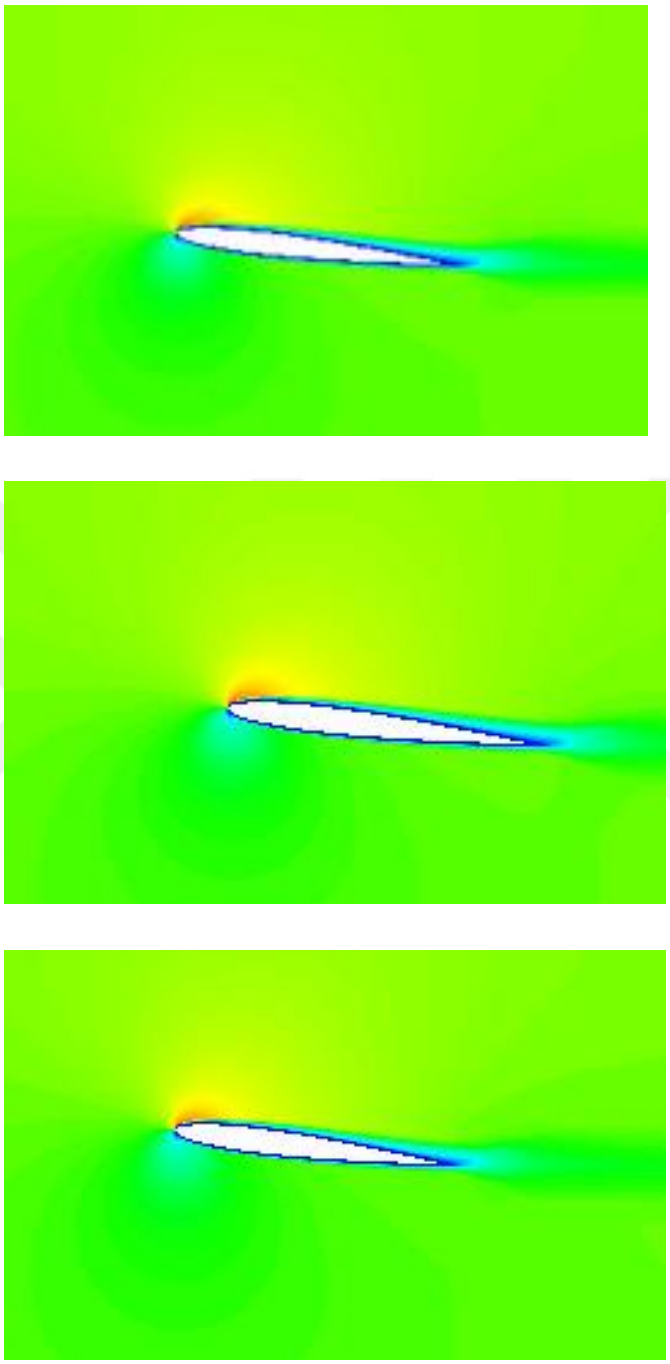

Figure 4.8: Velocity Profile of NACA 0009 at 7^{o} with Different Velocities.

Pressure and velocity characteristics are clearly different in the charts. The figures show that the velocity separated and turbulence increased as the angle of attack increased. The pressure impact increased as well, as illustrated in the red areas. Sandia National Laboratories SNL released the standard numerical findings of the NACA 0009 airfoil, and Yasin Furkan GÖRGÜLÜ et al, 2021 [7] published the data.

At the same wind speed, wind turbine blades will have a larger lift force and torque, which will ultimately result in more electricity being generated. In wind turbines, an increase in the drag force causes the tangential force, which is responsible for producing torque, to decrease while the axial force, which is responsible for pushing the blades backward and does not contribute to power production, rises. The relationship between the lift coefficient and the angle of attack is seen in figure 8. The angle of attack continues to climb until it reaches 10 degrees, at which point the lift achieves its maximum intensity. The lift coefficient reaches its highest point at this point, and then drops to 0.661.

The simulation results of NACA 0009 at velocity = 5 m/s of lift coefficient and drag coefficient are presented in the tables below, based on the aforesaid factors.

Table 4.1: Lift Coefficient Comparison

A.O.A	Previous studies [7]	Present study Results	Percentage Error
0	0.000001	0.00093	0
5	0.461	0.473749	2.77%
7	0.65	0.624	4.00%
10	0.748	0.724016	3.21%
15	0.661	0.6731	1.83%

In all applications, including wind turbines and aircraft, drag is an unwelcome force acting against the moving item. Maintain it at the very minimal practical level. Figure 9 depicts how an increasing attack angle results in a constantly increasing drag force. When the angle of attack is 15 degrees, the coefficient of drag reaches its highest value of 0.24439.

Table 4.2: Drag Coefficient Comparison

A.O.A	Previous studies [25]	Present study Results	Percentage Error
0	0.01742	0.0192	---
5	0.04597	0.04499	2.13%
7	0.07192	0.07211	0.26%
10	0.10172	0.09919	2.49%
15	0.24439	0.2511	2.75%

The results show that variations in angle of attack have an impact on the drag coefficient and force coefficient. Figures 4.9 and 4.10 show the results of the CFD simulation in order to better understand the behavior.

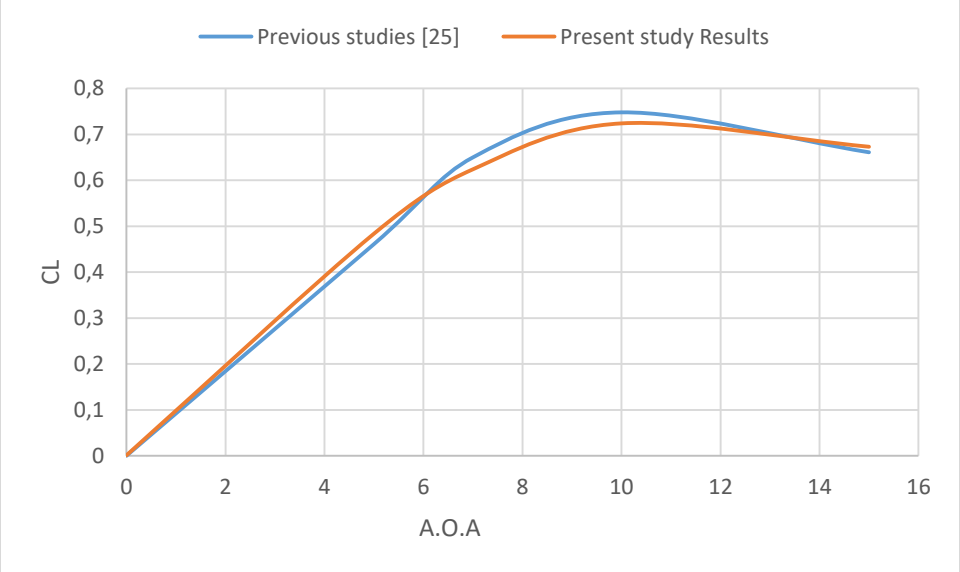

Figure 4.9: Lift Coefficient Comparison Result.

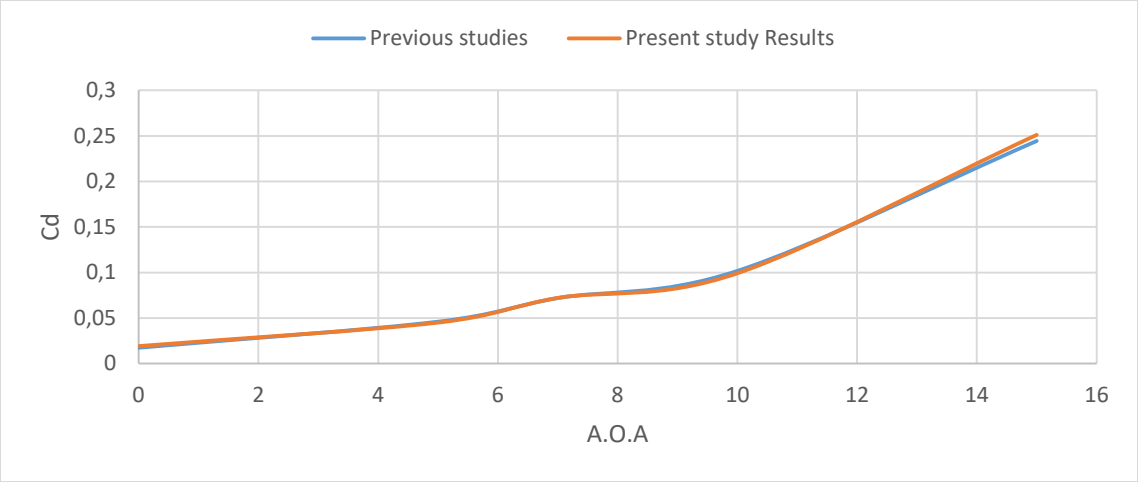

Figure 4.10: Drag Coefficient Comparison Result.

Due to the close proximity of the curves, we may conclude that the CFD ANSYS model is credible.

When it comes to lift, the greater the value, the better; when it comes to drag, the lower the value, the better. When the angle of attack is 10 degrees, the lift coefficient achieves its maximum value of 0.748, while the drag coefficient reaches its minimum value of 0.01742. According to the statistics, it is impossible to determine which type of attack has the greatest likelihood of success or which of the several possible tactics will be used. As a result of this, the lift-to-drag ratio must be calculated. The ratio of lift to drag (L/D) is seen in Figure 4.11. This graph, which shows a ratio of 10.03, illustrates that a 5-degree angle of attack yields the greatest results.

Table 4.3: Comparison of L/D Results.

A.O.A	Previous studies	Present study Results	Error %
0	5.7405E-05	0.0484375	0
5	10.0282793	10.53009558	5.00%
7	9.0378198	8.653446124	4.25%
10	7.35351947	7.299284202	0.74%
15	2.70469332	2.680605337	0.89%

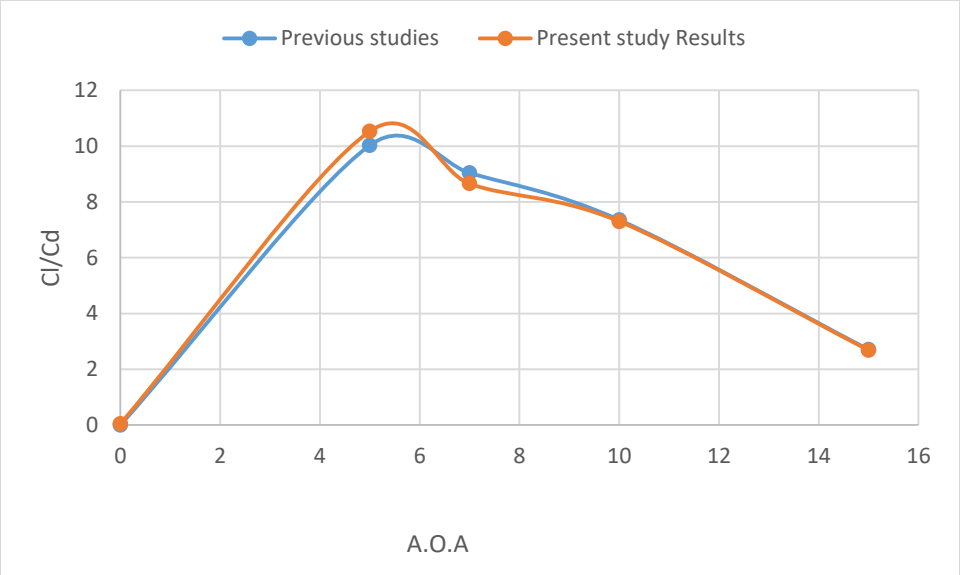

Figure 4.11: Plot of L/D results for NACA 0009.

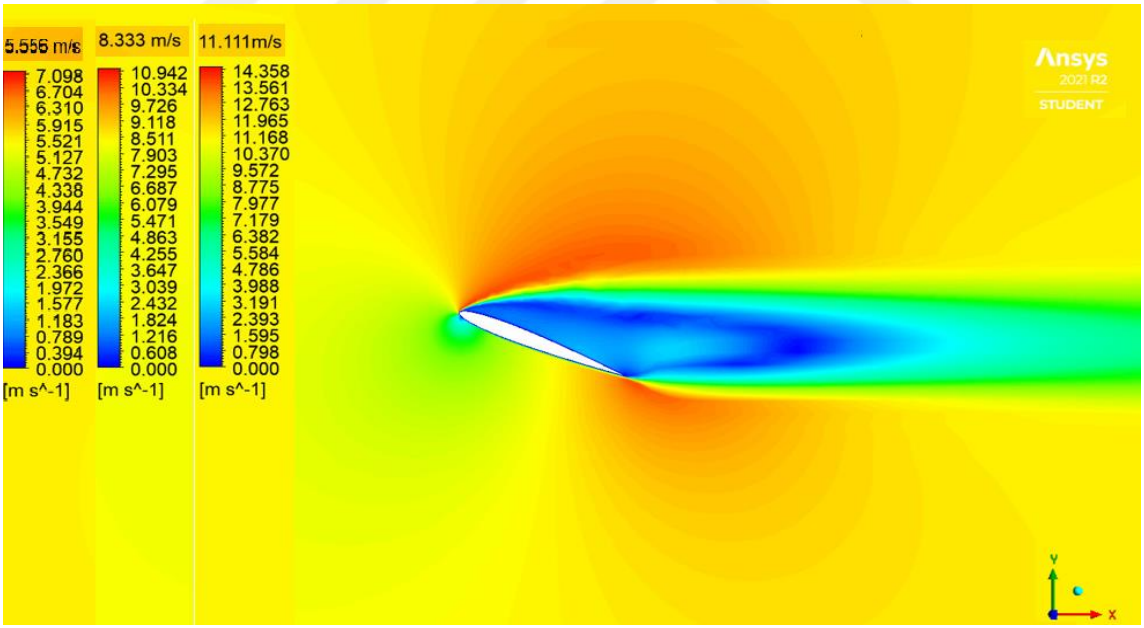

Figure 4.12: Velocity Profile at 15^{o}.

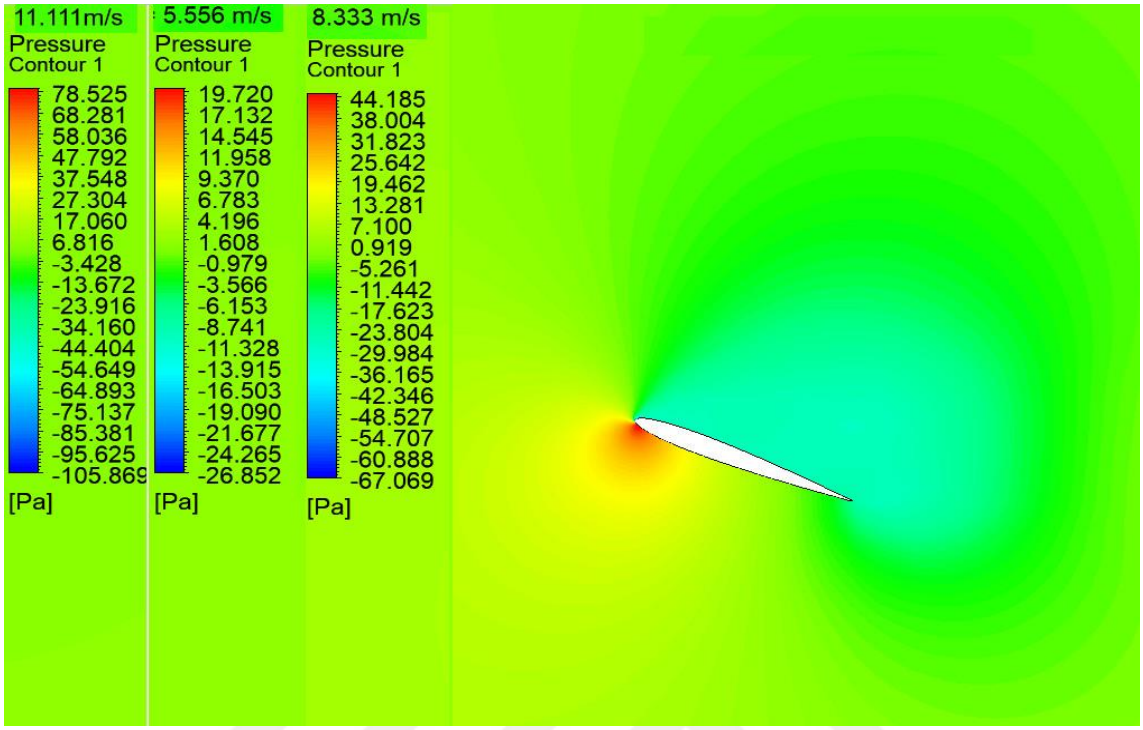

Figure 4.13: Pressure Profile of 15°.

Table 4.4: Comparison of C_L Results with Different Velocities of NACA 0009.

A.O.A	V = 5.5 m/s	V = 8.33 m/s	V = 11.11 m/s
0	0.00093	0.0009579	0.000937
5	0.483749	0.50793645	0.533333
7	0.624	0.64896	0.674918
10	0.724016	0.92674048	1.186228
15	0.6731	0.861568	1.06202527

Table 4.5: Comparison of C_D Results with Different Velocities of NACA 0009.

A.O.A	V = 5.5 m/s	V = 8.33 m/s	V = 11.11 m/s
0	0.0192	0.019776	0.020369
5	0.04399	0.0461895	0.048499
7	0.07311	0.0760344	0.079076
10	0.09919	0.1269632	0.395579077

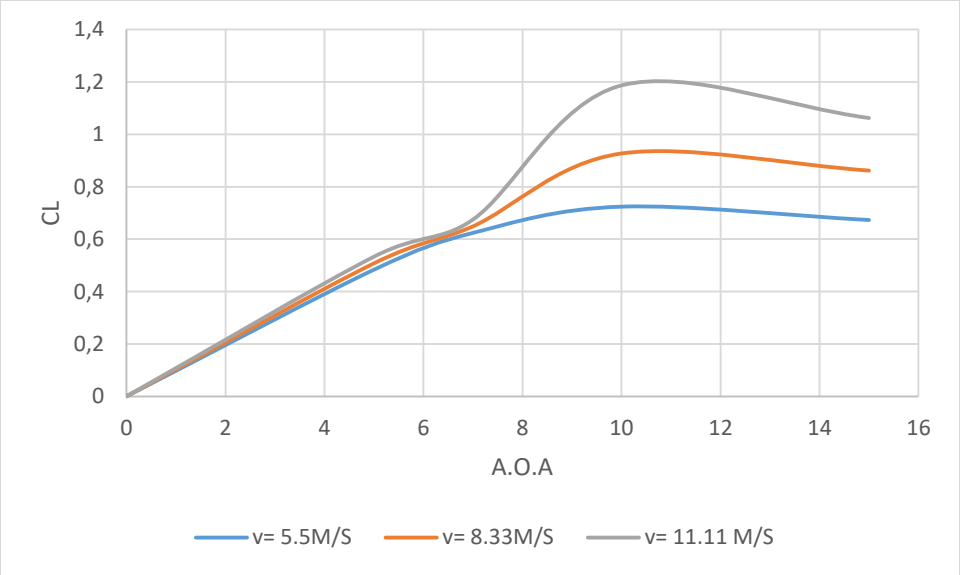

Figure 4.14: Comparison Plot of C_L Results with Different Velocities of NACA 0009.

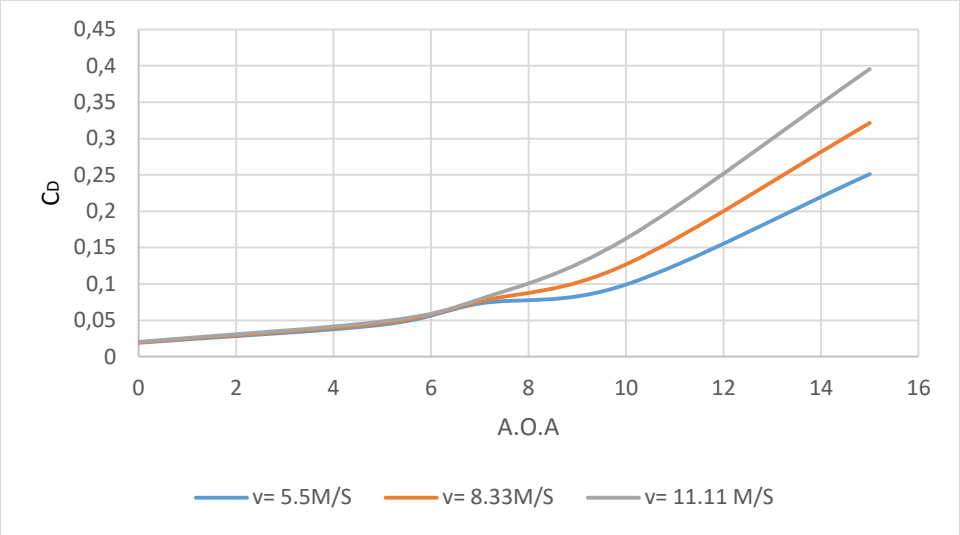

Figure 4.15: Comparison Plot of C_L Results with Different velocities of NACA 0009.

4.2 AERODYNAMIC ANALYSIS OF S1223

Aerodynamic properties were investigated using the ANSYS solver and a wing design of S1223. AoA has a range of 0 to 15 degrees. Figures 4.6 and 4.7 illustrate the CFD ANSYS findings for the zero-angle employed in turbulence shear stress transfer (SST) k- and 5.5 m/s. The velocity and pressure distributions on the wing surface are found to be convergent on both sides of the wing. The maximal pressure effect may be seen in the red color of the pressure profile at the

wingtip. Because the impacted force component could not be applied perpendicularly on the longitudinal axis of the wing section, this notice certifies that there is no effective lift force in this angle degree. Changes in angle of attack have altered the properties of the airfoil.

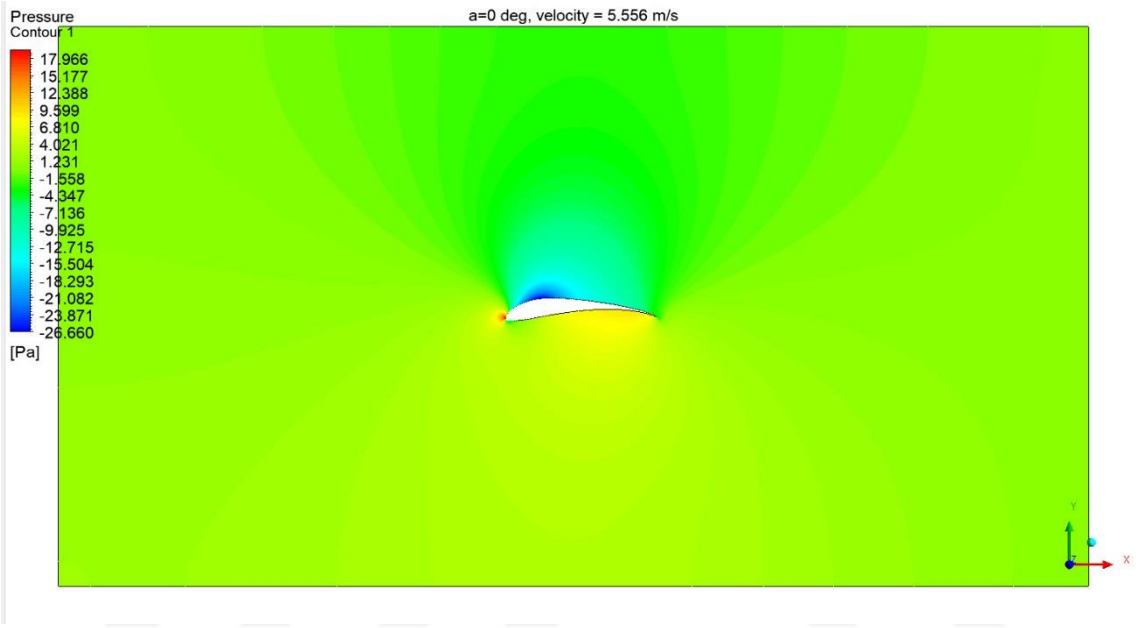

Figure 4.16: Pressure Contour Result of CFD Run of S1223 wing section, v= 5.5 m/s. Angle 0^{o}.

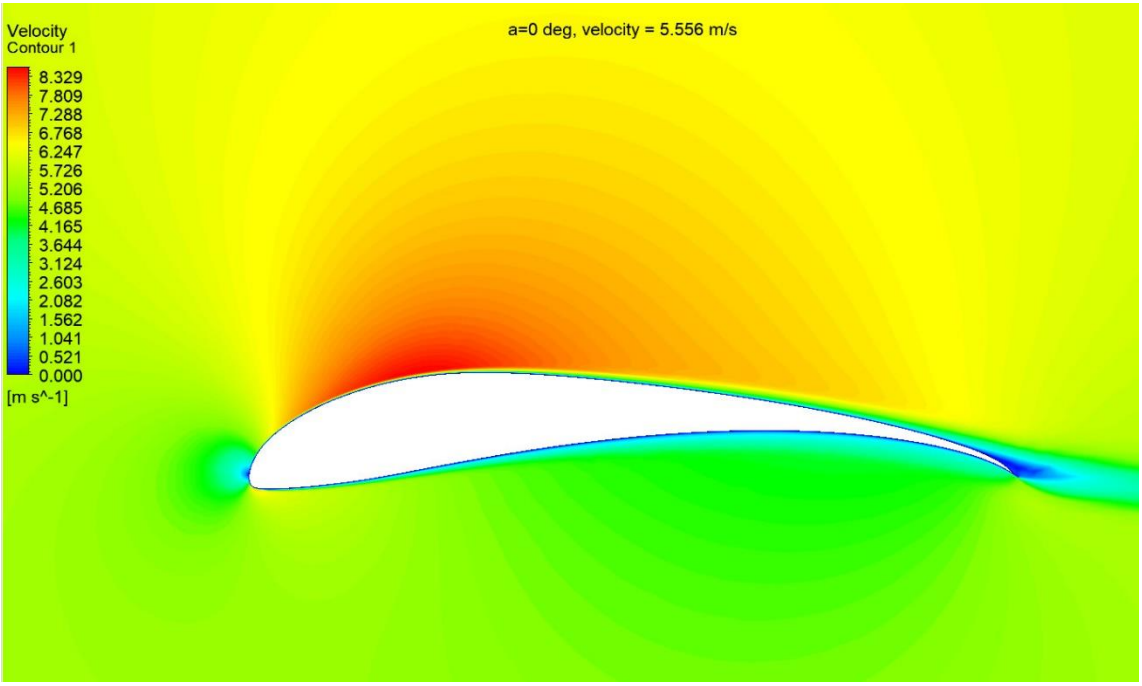

Figure 4.17: Velocity Contour Result of CFD Run of S1223 wing section, v= 5.5 m/s. Angle 0^{o}.

As a result, the ANSYS simulation increased the angle of attack based on two degrees of variance and observed the following set of results:

a) As demonstrated in the red zone, the velocity contours reveal an increase in air speed in the top surface of the wing and a drop in the bottom surface. Because the lift force and air speed at the top surface of the wing have an inverse relationship, the lift force will rise in this instance.
b) When attacking from a higher angle, a vortex will appear. The drag force will be increased by the vortex. Figure 4.18 shows the findings from four distinct viewpoints.

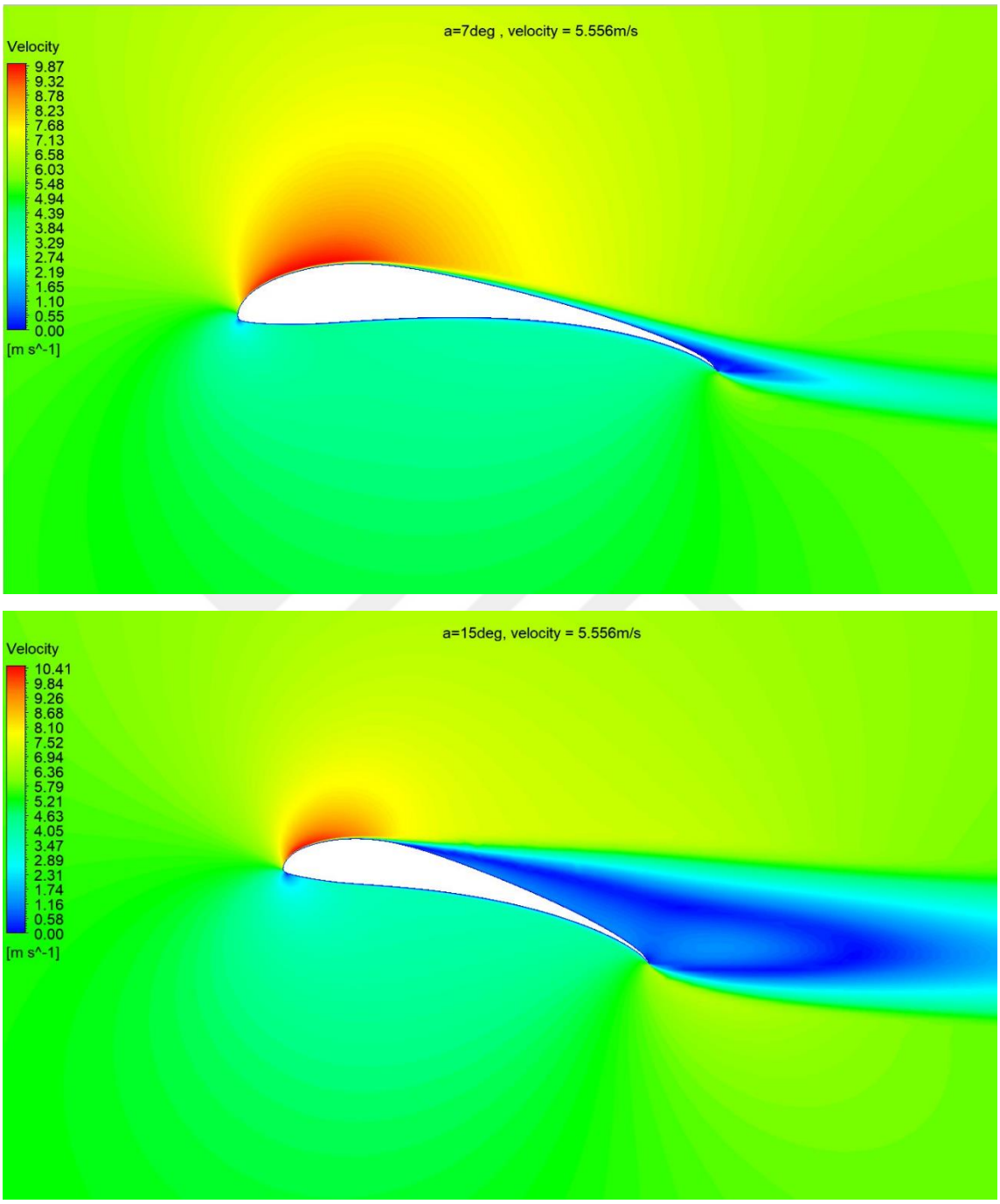

Figure 4.18: The Velocity Contours Results of S1223 Wing Section.

c) As demonstrated in the red zone, the pressure contours reveal a rise in the bottom surface of the wing and a drop in the upper surface. Because there is a positive connection between lift force and air pressure at the upper and lower surface of the wing, this finding implies that there is resistance against the flow direction, implying that the lift force will grow.

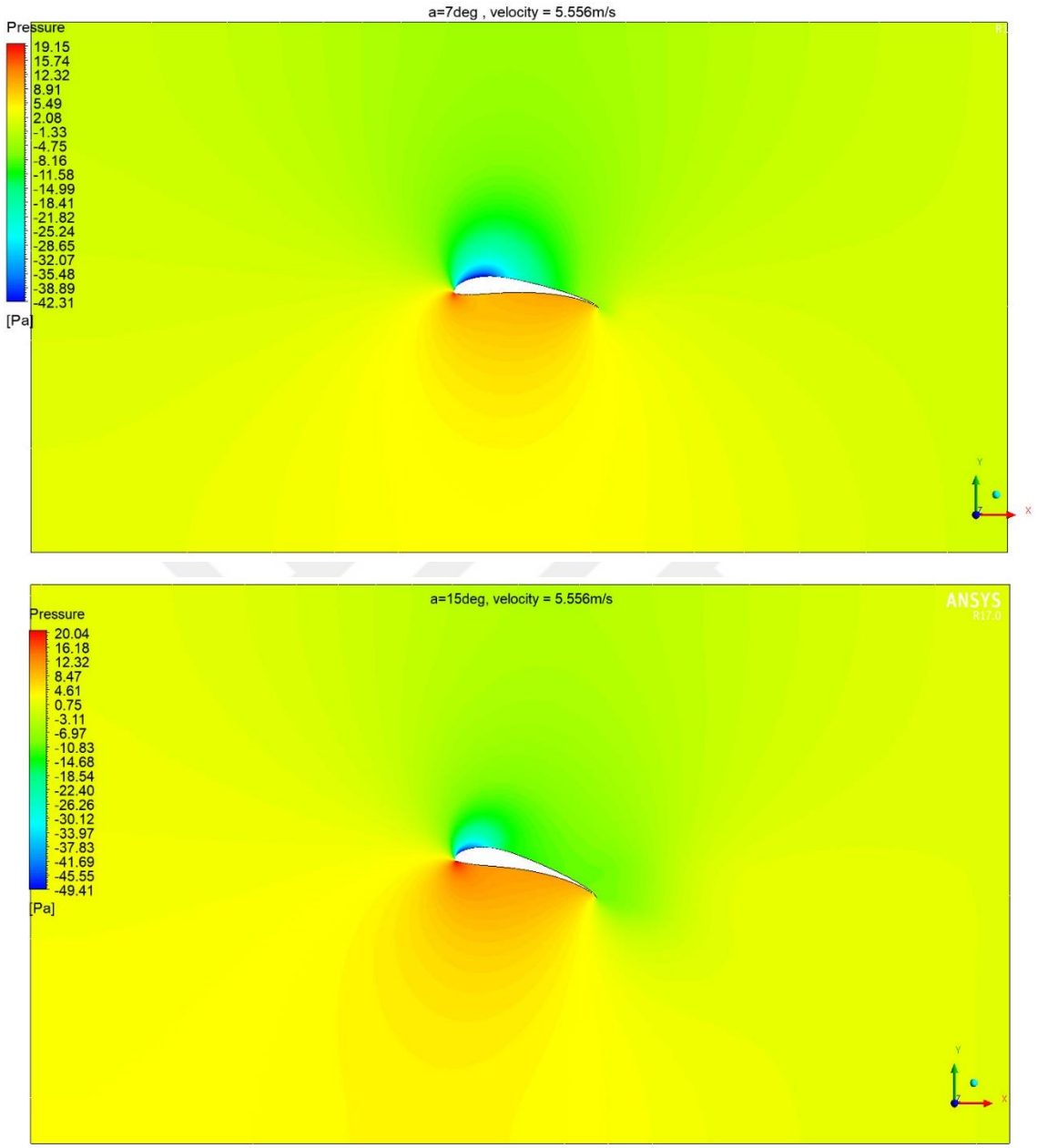

Figure 4.19: The Pressure Contours Results of S1223 Wing Section.

4.2.1 Numerical Results of S1223

The compilation of aerodynamic values is available in the numerical output generated by ANSYS -FLUNT procedures. These figures illustrate that the angle of attack has a considerable effect on both the lift forces and the drag. In the usual technique, the airfoil's geometry is represented using meshing, and the National Advisory Committee for Aeronautics is responsible

for data collection (NACA). Throughout the whole scenario, the assault angle fluctuated between 0 and 15 degrees. These statistics are derived from the results of the airfoil simulation and then split down into lift, drag, and coefficients. In table 4.6, the results of the lift force lift coefficients and drag coefficients are tabulated with their corresponding numerical representations. The major objective of the S1223 wing, according to the results, is to produce a stronger lift force. As a result, the shape of the wing has been selected because it is believed to be the most ideal for directing the airflow via physical activity.

Table 4.6: Numerical Results of S1223

AoA	CL	CD	CL/CD
0	1.2	0.025	48
5	1.7	0.028	60.71429
7	1.9	0.033	57.57576
10	2.2	0.047	46.80851
15	2.1	0.078	26.92308

The results show that when the angle of attack is increased, the lift force increases progressively. These findings show that the force values rise dramatically between angles of 5o and 10o. Because of the distinctive bottom surface design, air flow in the front bottom of the wing was restricted.

The properties of the air layers around the wing surface are the reason for increasing lift force. Changes in the air molecules' stickiness to the wing surface modified the boundary layers of air flow behavior. Any item moving through a gas causes this effect. The gas's viscosity (or stickiness) may detach from the body, resulting in a new boundary layer form that differs from the original. In this instance, the boundary layer is unstable and becomes turbulent at random. It's also worth noting that the curvature grows until the 10th degree of attack angle. This angle represents the stall angle and specifies the maximum airfoil angle of the aircraft wing that can be allowed.

The Lift and Drag Coefficients are aerodynamic numbers that represent the intricate relationships between form and inclination. For this reason, the Lift and Drag Coefficients were investigated and compared in this study. As a function of lift force, air velocity, air density, and wing surface area, the lift coefficient is calculated. This definition applies the lift coefficient notion to the dynamic pressure of an airfoil. The lift coefficient is determined by these characteristics. The drag coefficient impact is also taken into account in the same notion. The lift and drag coefficients are calculated using numerical findings. In both situations, the increases are gradual as the angle of attack is increased. That means the lift and drag coefficients accurately represent the wing's real acting forces. We may deduce from these facts that the lift and drag, which constitute the aircraft's design consideration, are dependent on the lift and drag coefficients for any item. Due to the lift force created by air speed, the CFD simulation results of lift coefficient and drag coefficient, which includes the angle of attack variations influence, have been discovered. The clean wing is the most important requirement in this study. Many factors were also taken into account, such as the absence of rain and the constants of air temperature and humidity. Figure 4.20 shows a plot of lift and drag coefficients that shows how the forces coefficients vary as the AoA varies.

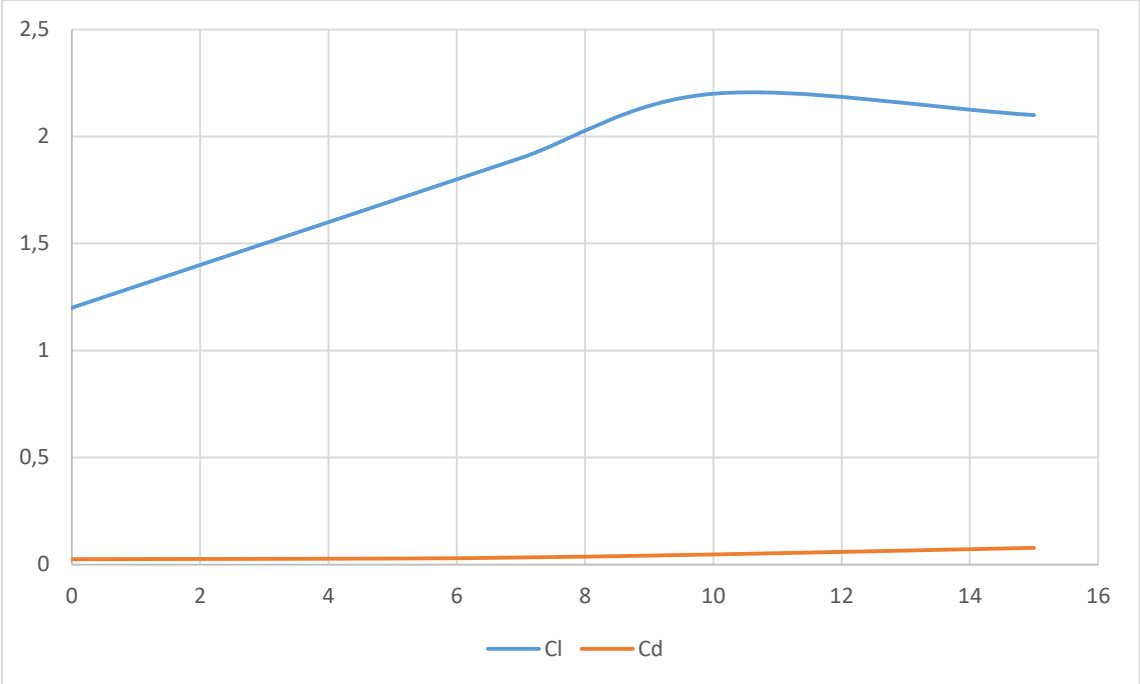

Figure 4.20: The Lift and Drag Coefficients of S1223.

Both the lift and drag coefficient values show a linear progression in the graph. The 10th degree of assault angle was the boundary line. Vortex lines extend from the wing tip due to air flow on the wing surface. A downwash of air is produced by the vortex line, which is illustrated as a blue vortex region. The findings demonstrate the downwash (a) as a consequence of this research and (b) as actual airplane downwash.

Vortex lines create air downwash, which is a significant concern for airplane lift and stability. As a result, preventing downwash is a crucial issue in airplane design, which takes into account the stall angle of attack as well as the drag value impact.

4.3 AERODYNAMIC ANALYSIS OF S1223 RTL

Aerodynamic properties were investigated using the ANSYS solver and a 3D wing configuration of the S1223 RTL. This procedure takes into account the same range of AoA. Figures 4.21 and 4.22 illustrate the CFD ANSYS findings for the angle of turbulence shear stress transport (SST) k- and 5.5 m/s.

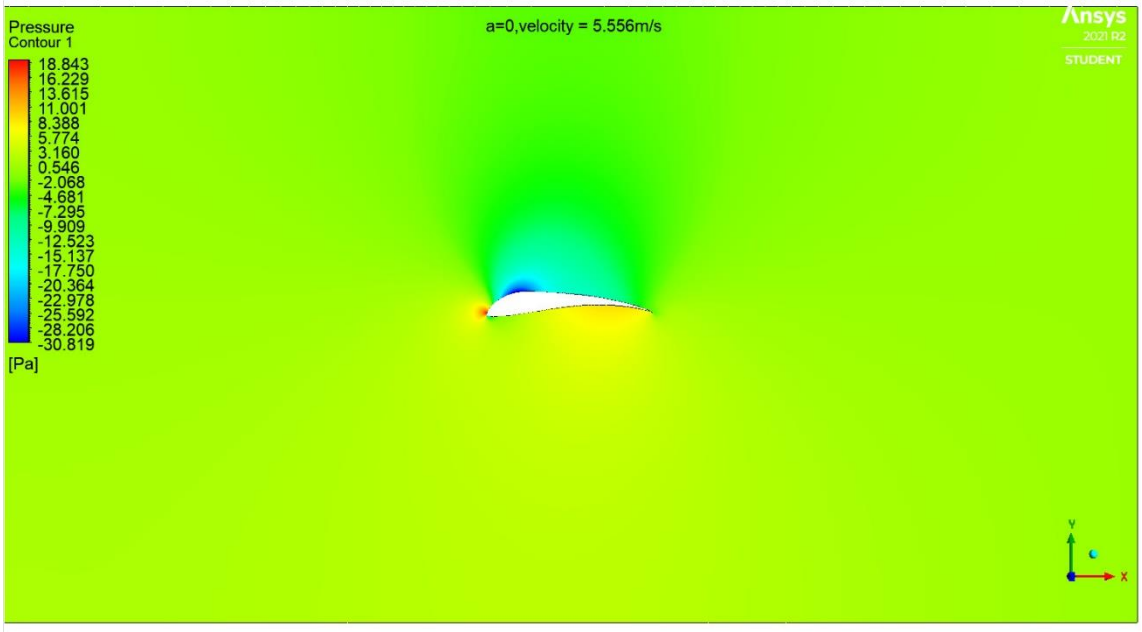

Figure 4.21: Pressure Contour Result of CFD Run of S1223 RTL Wing Section, Re 5.5 m/s. angle 0^{o}.

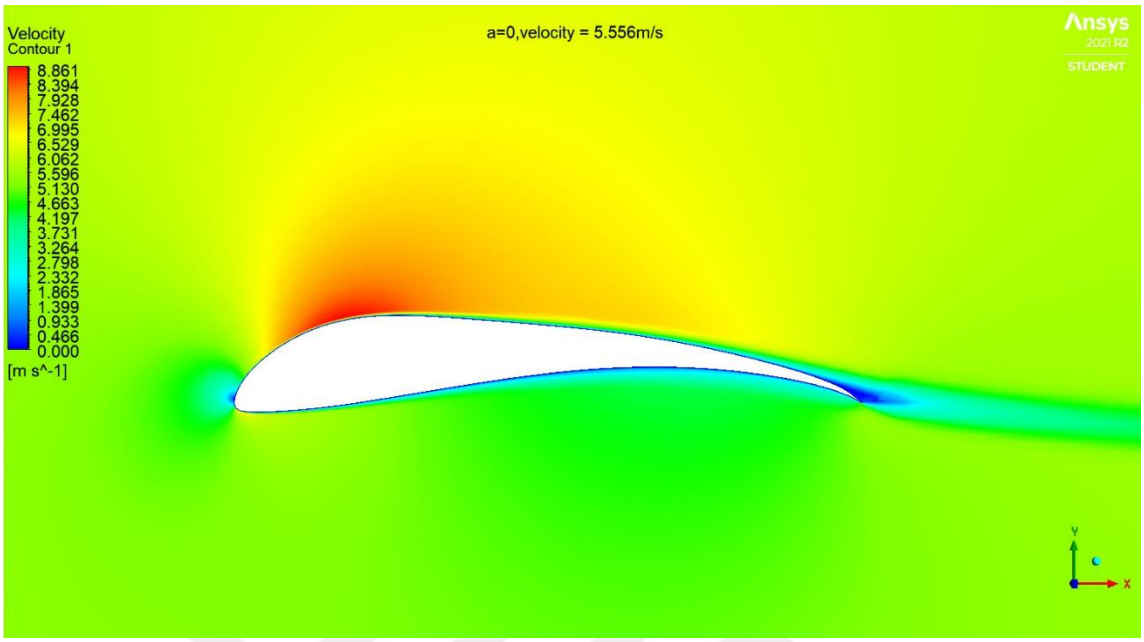

Figure 4.22: Velocity Contour Result of CFD Run of S1223 RTL Wing Section, Re 5.5 m/s. Angle 0^{o}.

a) The maximum pressure has an effect on the tip of the wing, as demonstrated by the red colour of the pressure profile. As previously stated, changes in angle of attack modified the airfoil properties; as a consequence, the ANSYS simulation applied an increase in angle of attack based on two degrees of variation and observed the following set of results:

b) Because the lift force and air speed in the upper surface of the wing have an inverse relationship, an increase in lift force is caused by an increase in upper surface air speed and a reduction in lower surface air speed.

c) The 10th AoA is the effective angle of attack.

d) As illustrated in the red zone, the pressure contours reveal a rise in the bottom surface of the wing and a drop in the top surface. The lift force is increased by the resistance against the flow direction due to the positive connection between the lift force and the air pressure in the upper and lower wing surfaces.

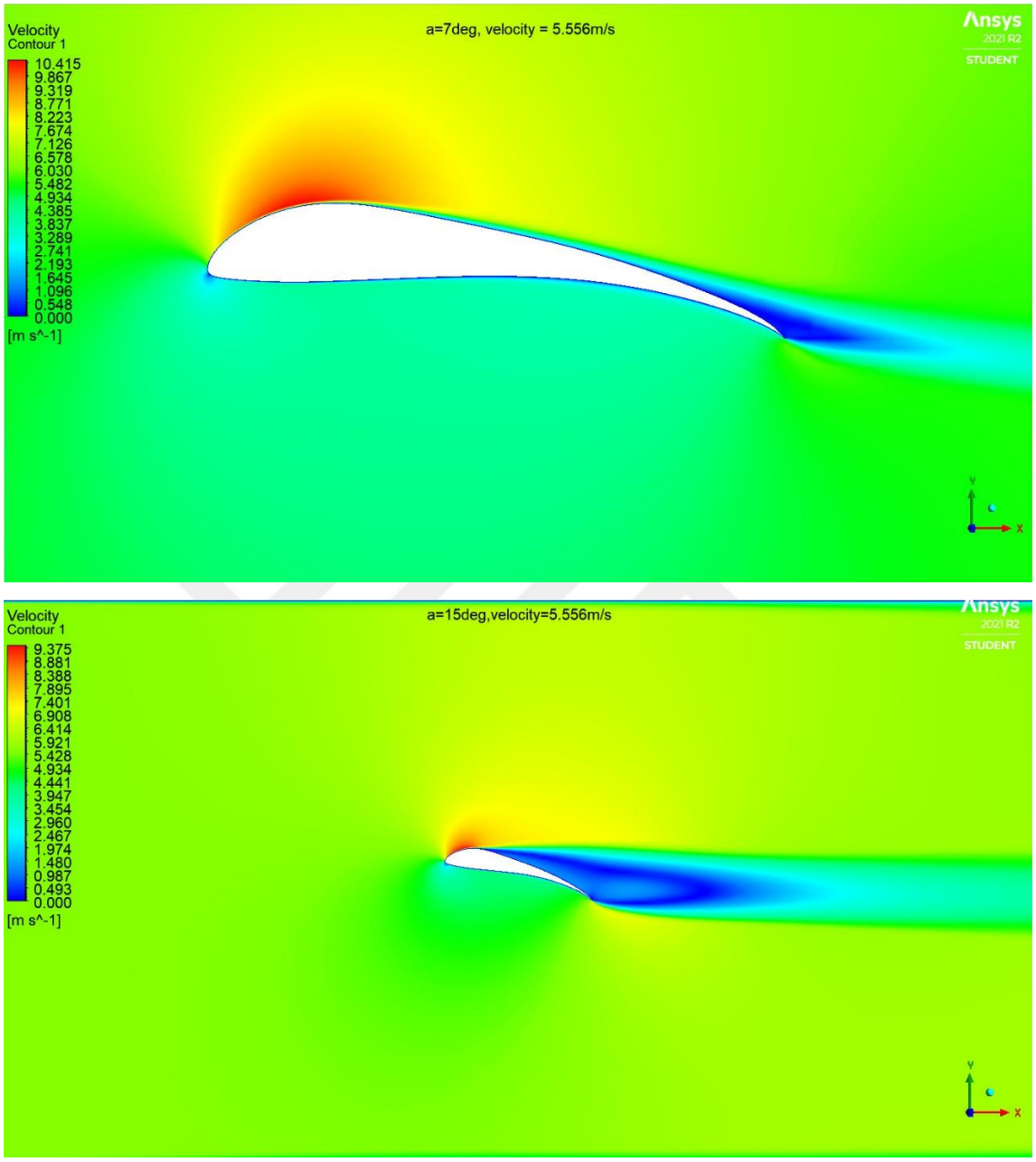

Figure 4.23: The Velocity Contours Results of S1223 RTL Wing Section.

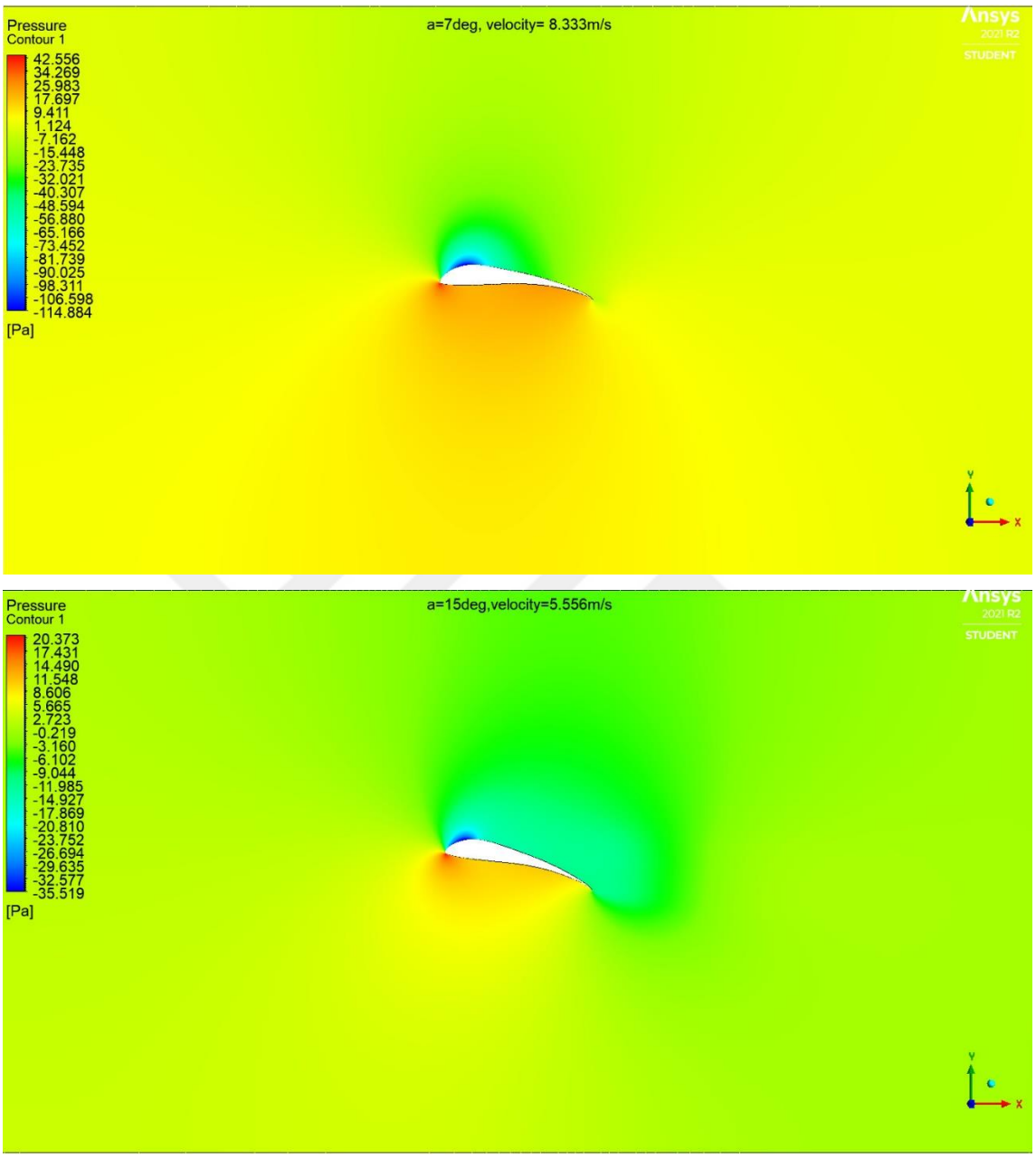

Figure 4.24: The Pressure Contours Results of S1223 RTL Wing Section.

4.3.1 Numerical Results of S1223 RTL

The numerical results for the S1223 RTL were derived using the same sequence as the prior model. The lift, drag force, and coefficients are resolved in the simulation run that employed the identical angles of attack as the airfoil simulation. The findings of the lift force lift coefficients and drag coefficients are shown numerically in Table 4.7. The major mission for the S1223 RTL wing, based on the findings, is to examine the forces' behavior. As a result, the chosen wing form is thought to be suited for turning air flow through physical movement.

Table 4.7: Numerical Results of S1223 RTL

AoA	CL	CD	CL/CD
0	1.37	0.022	62.27273
5	1.79	0.024	74.58333
7	1.96	0.031	63.22581
10	2.27	0.042	54.04762
15	2.124	0.073	29.09589

The findings reveal that the lift force grows progressively as the angle of attack increases, as shown in the prior model. The results reveal a link between the increase in angle of attack and the rise in lift force impact. The properties of the air layers around the wing surface cause the lift force to rise for the same reason. As previously stated, the boundary layers of air movement behavior varied due to changes in air molecules sticking to the wing surface, causing unstable and unpredictable turbulence behavior.

The lift and drag coefficients are used to represent the shape characteristics, which are connected with flow conditions and inclinations. The lift and drag coefficients were researched and compared in this study. The lift coefficient is calculated using lift force, air velocity, air density, and the wing's surface area. This definition applies lift coefficient principles to airfoil dynamic pressure. The lift coefficient is determined by these characteristics. The drag coefficient impact is also taken into account in the same notion. The lift and drag values are determined by the

numerical findings. In both circumstances, the increases are gradual as the AoA grows. This means that the lift and drag coefficients accurately represent the wing's real acting forces. We may deduce from these facts that the lift and drag, which constitute the aircraft's design consideration, are dependent on the lift and drag coefficients for any item. The lift and drag coefficients connected with air speed were observed in the CFD results of the analyzed parameters. The wing form is the most basic criterion in this study. Many factors were also taken into account, such as the absence of rain and the constants of air temperature and humidity. Figure 4.25 shows a plot of lift and drag coefficients that shows how the forces coefficients vary as the AoA varies.

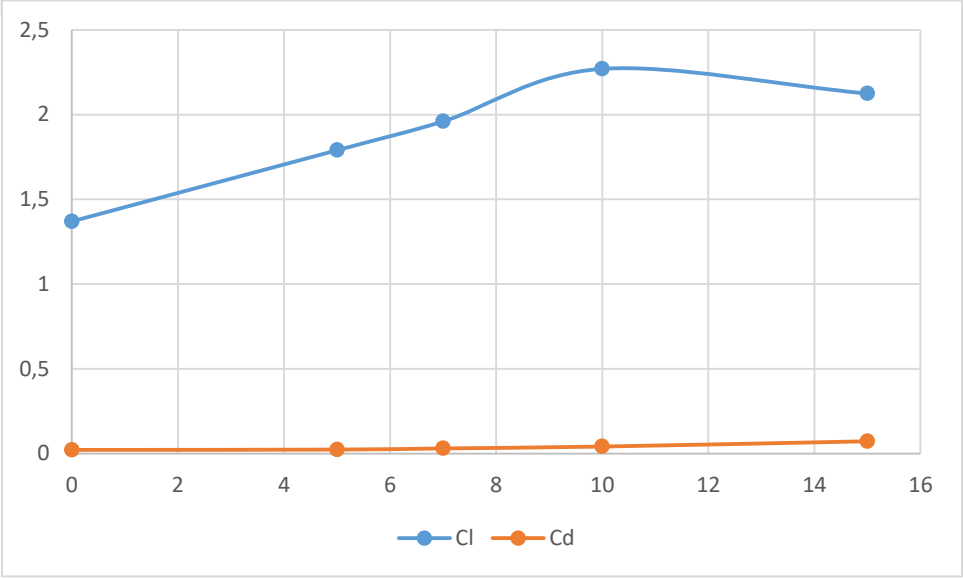

Figure 4.25: Lift and Drag Coefficients of S1223 RTL.

The lift coefficient curve has a semi-linear progression, while the drag coefficient line has a linear progression. The 10th degree of assault angle was the boundary line. In this model, the sane phenomena were seen. Vortex lines extend from the wing tip due to air flow on the wing surface. Apart from the drag value impact, air downwash caused by vortex lines is managed by considering the stall angle of attack, which is the maximum wing angle. This phenomenon is regarded as a critical issue in the field of airfoils.

4.4 AERODYNAMIC OPTIMIZATION OF AIRCRAFT

It is clear from the results that the S1223 RTL wing has less pressure value in the top surface than the S1223 type. Therefore, the lift force in S1223 RTL became higher.

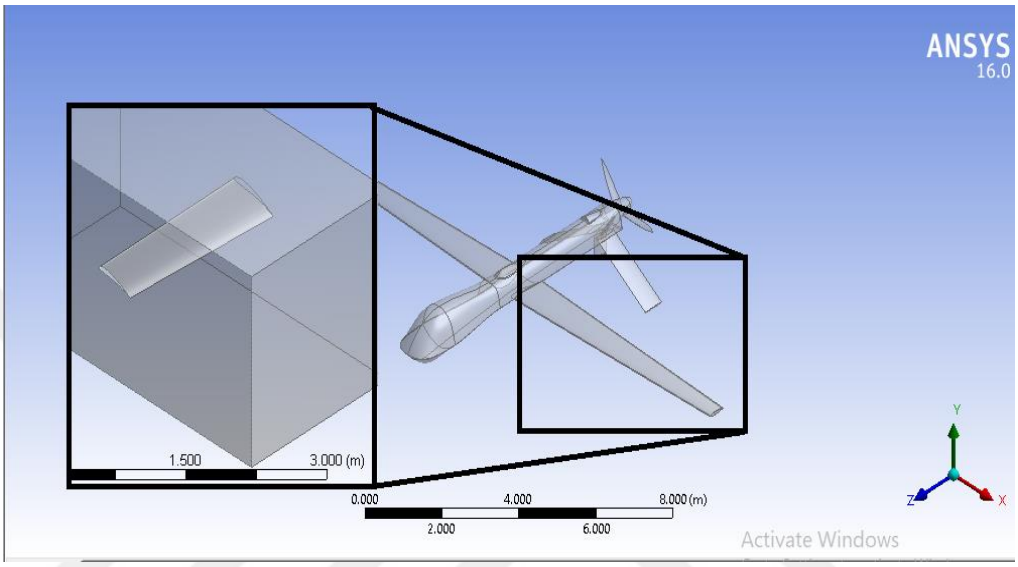

Figure 4.26: 3D Plot of the Wing Shape.

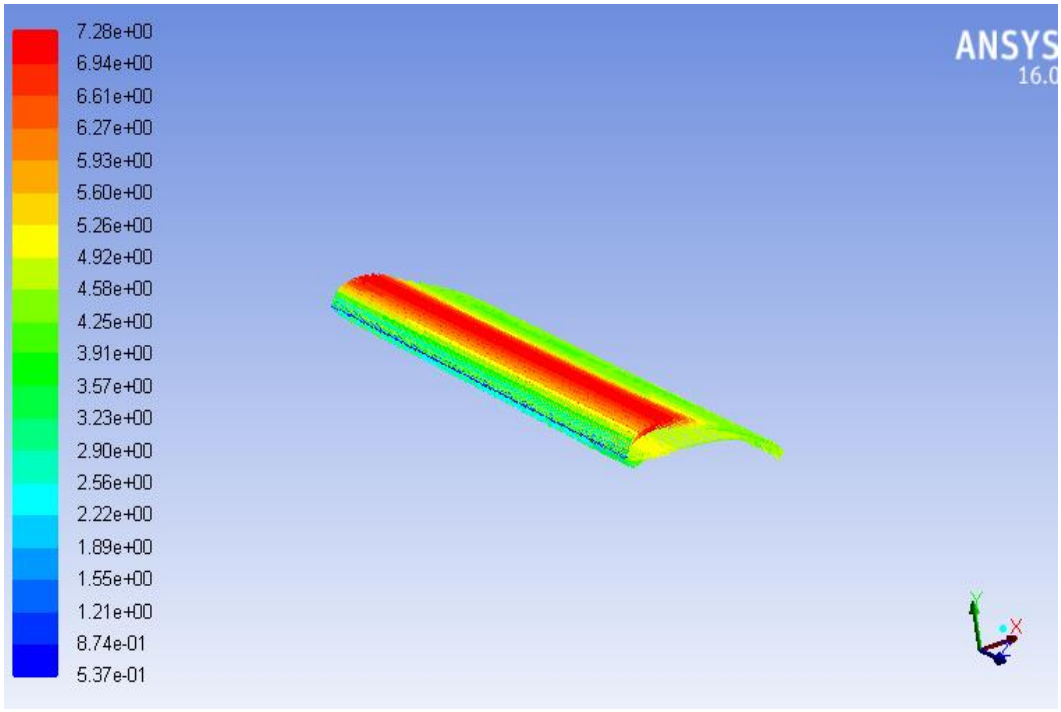

Figure 4.27: Simulation of 3D Wing Shape.

The lift coefficient value depends on the coefficient of pressure. The correlation can be derived from the formula below:

$$C_L = \frac{1}{c}\int_0^c \left(C_{p,L} - C_{p,U}\right)dx \qquad 4.1$$

where c is the chord length and Cp and Cp are the pressure coefficients on the airfoil's lower and upper surfaces, respectively. The region encompassed by the difference in pressure coefficients is known as the coefficient of lift. The dimensionless quantity known as the coefficient of pressure describes the pressure distribution over the surface of the airfoil.

$$C_p = 1 - \left(\frac{V}{V_\infty}\right)^2 \qquad 4.2$$

Where V∞ is the free stream velocity and V is air velocity at the same point.

Due to the fact that lift is a kind of aerodynamic force, it is affected by changes in air pressure as the body passes through it. Lift force and lift coefficient discrepancies are caused by variances in air speed between the top and lower surfaces due to differing AoA and wing area. The capacity of wings is determined by the variations in upper and lower pressure and velocity levels.

The amount of lift created is proportional to the object's size. The overall aerodynamic force is equal to the pressure multiplied by the surface area around the body. A force that is perpendicular to the direction of flight is referred to as "lift." When the object's surface area is increased, so does the lift's power output. S1223 RTL wing's lift force and lift coefficient are improved by expanding the wing area. The drag coefficient shows the same effect. The flow created by the vortex pair that makes up the wake has a significant impact. In the free-stream ahead of the wing, a downward velocity component is produced by the semi-infinite sheet of vorticity spread in the wake.

A comparative investigation and analysis are presented in this study to examine the outcomes in order to understand the airfoil behavior based on different types of wing sections. Table 4.8 shows the technical comparison of the selected airfoils.

Table 4.8: Comparison and Optimization of the Selected Wings

	S1223	S1223 RTL
Wingspan	3m	3m
Wing Area	2.196	2.196
min velocity	8.4 m/s	8.2m/s
lift load	233.3388	240.7633
UAV wieght	20kg	20kg
flight time	8 hrs	8.195hrs

4.5 OPTIMIZATION OF S1223 WITH ADDING SOLAR POWER ENERGY

An aircraft's design is based on requirements that must be satisfied by the aircraft in question. The intended usage determines these criteria. A performance or contract specification is another name for a collection of requirements. The flying mission generates several needs. Aeronautical engineers can figure out an aircraft's shape by looking at how air flows around it. There are a number of factors that contribute to how air flows around an aircraft, including its wings, tail, and fuselage. Most fixed-wing and rotary-wing aircraft have traditionally been powered by hydrocarbon-fuelled internal combustion engines.

The capacity of a solar cell to create voltage and current in response to a load is what enables it to generate energy when irradiated by light [10,11]. As an illustration of this capacity, the graph (I - V) below depicts the relationship between current and voltage.

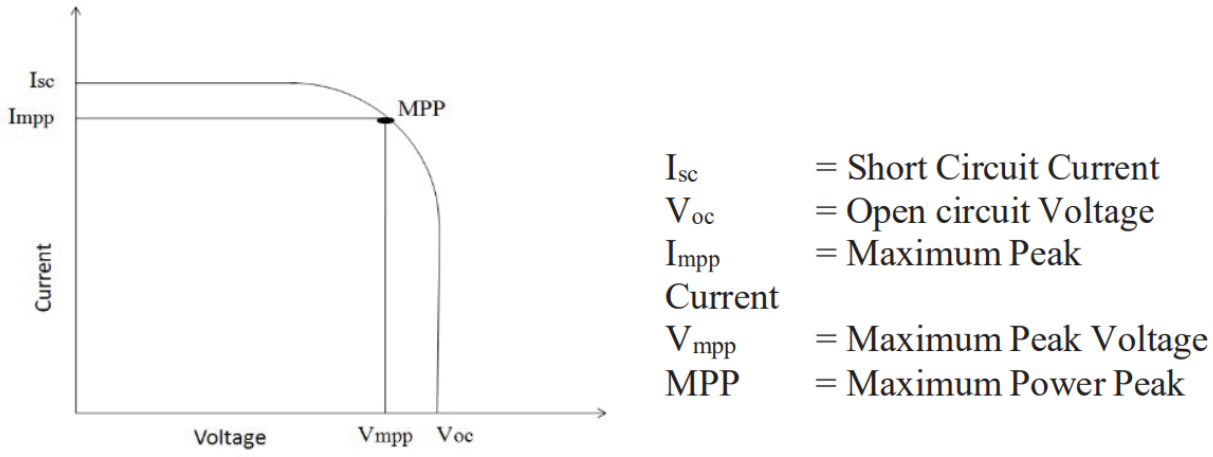

Figure 4.28: I-V Characteristics on solar cell.

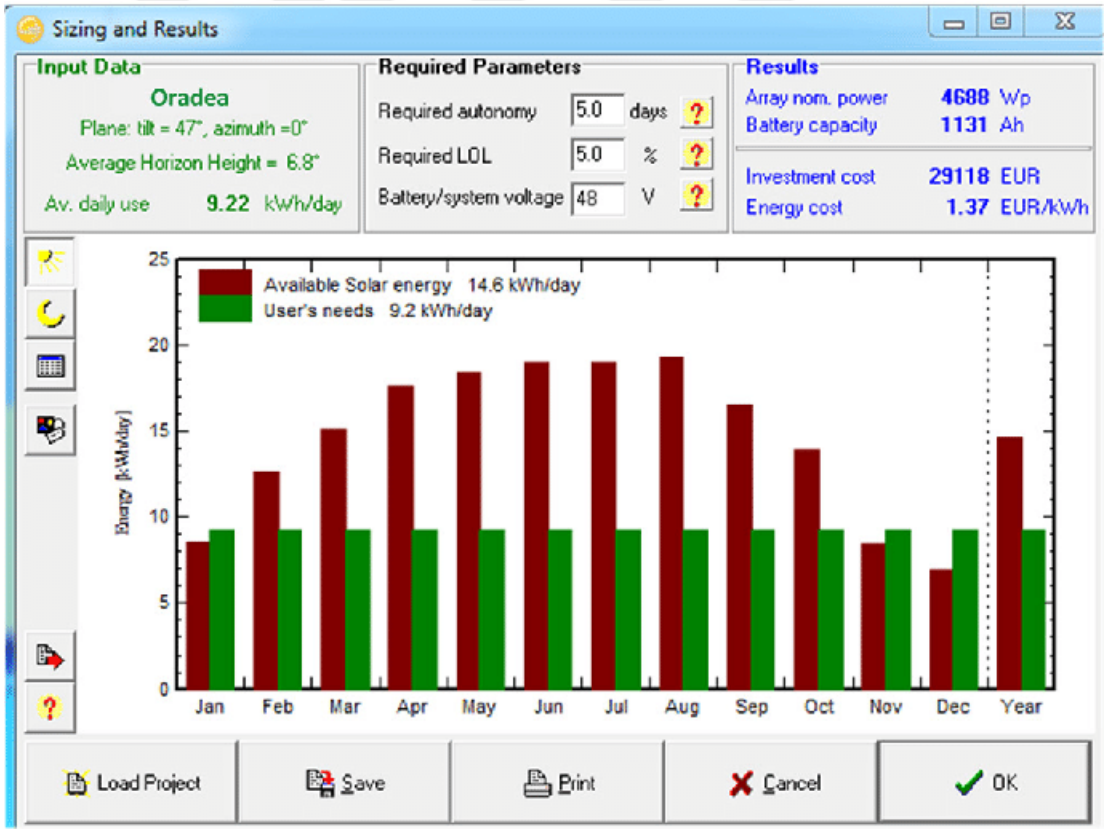

Figure 4.29: PVSYST calculation of the required number of cells and power output to cover the Flight system.

Table 4.9: PV system characteristics required for power coverage.

Cell Size	15cm*15cm
Pv voltage output	5v
Required workspace	1.5 m
Cell weight	4 grams
Number of cells	10

Due to the investigation's emphasis on electrical systems and solar cells, a fixed-wing unmanned aerial vehicle (UAV) is employed for this study. The choice of the fixed-wing design was based on the ability of its fuselage and wing to permit the placement of solar cells above the wings.

he assembled UAV and the corresponding component systems are shown in Figure 4.8. The Energy Storage System, Flight Control and Vital Electronic System are integrated into the fuselage. The UAV receives ground signals and makes attitude adjustments via transmitter and receiver.

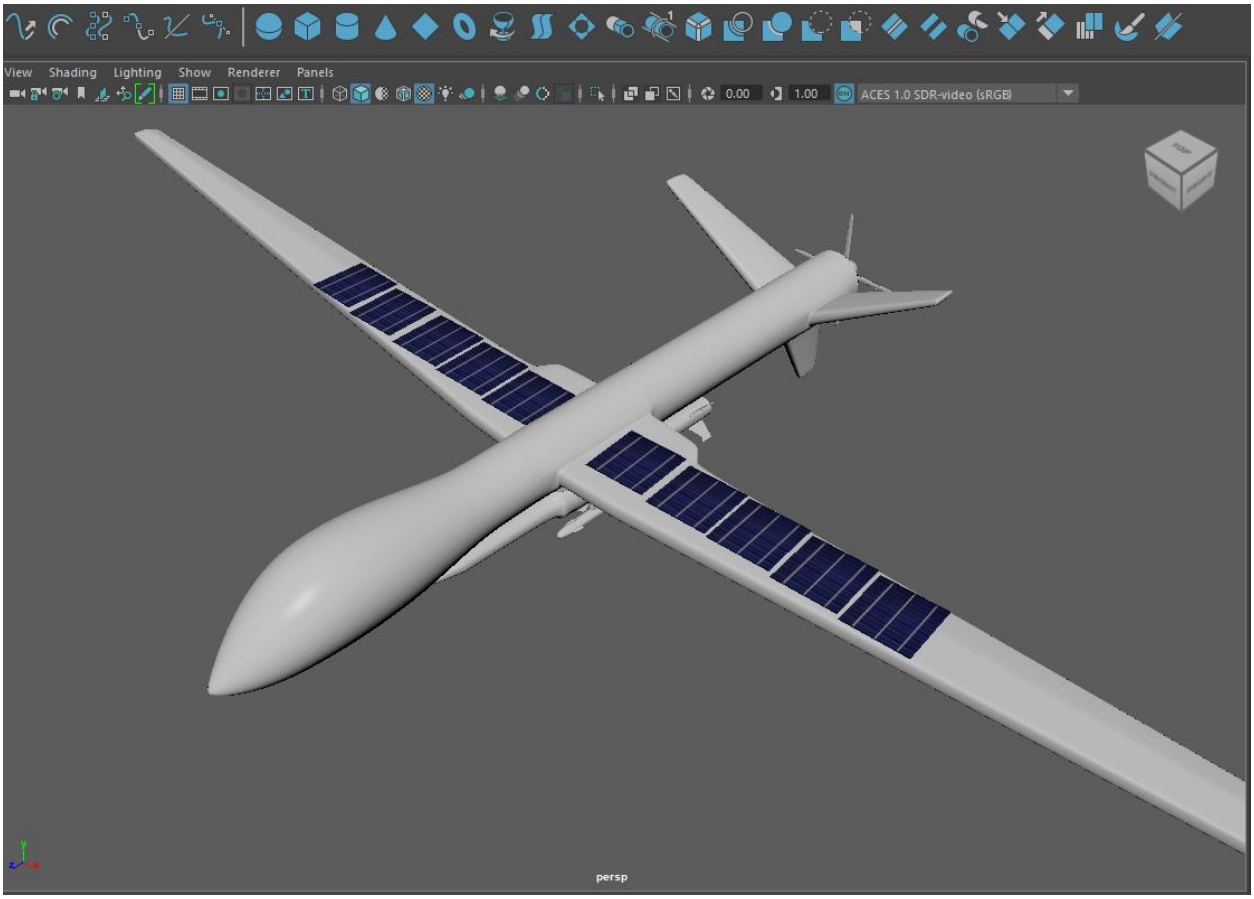

Figure 4.30: 3D design of the solar powered UAV.

The output power of a solar panel depends on the product of voltage and current, the Maximum Power Point Tracking (MPPT) circuit is designed to maximize the output power of the solar array in different light environments. Two sets of solar arrays were designed in this research, the solar panels on the upper wing will be directly exposed to the sun. Solar panels on the underwing receive direct light only in rare cases, such as forest fires, but most of the time receive diffuse light from the environment and the ground [47]. confirms that solar panels, especially bifacial solar panels, can absorb energy from the ground. The different ground shapes and materials reflect sunlight differently, which affects the efficiency of solar panels. This leads the researcher to consider supplying energy to some of the low energy circuits of the aircraft, such as the flight control module, by adding solar panels to the lower surface of the wing. Two separate MPPT circuits are necessary to maximize two sets of solar arrays since arrays will have different voltage-current curves.

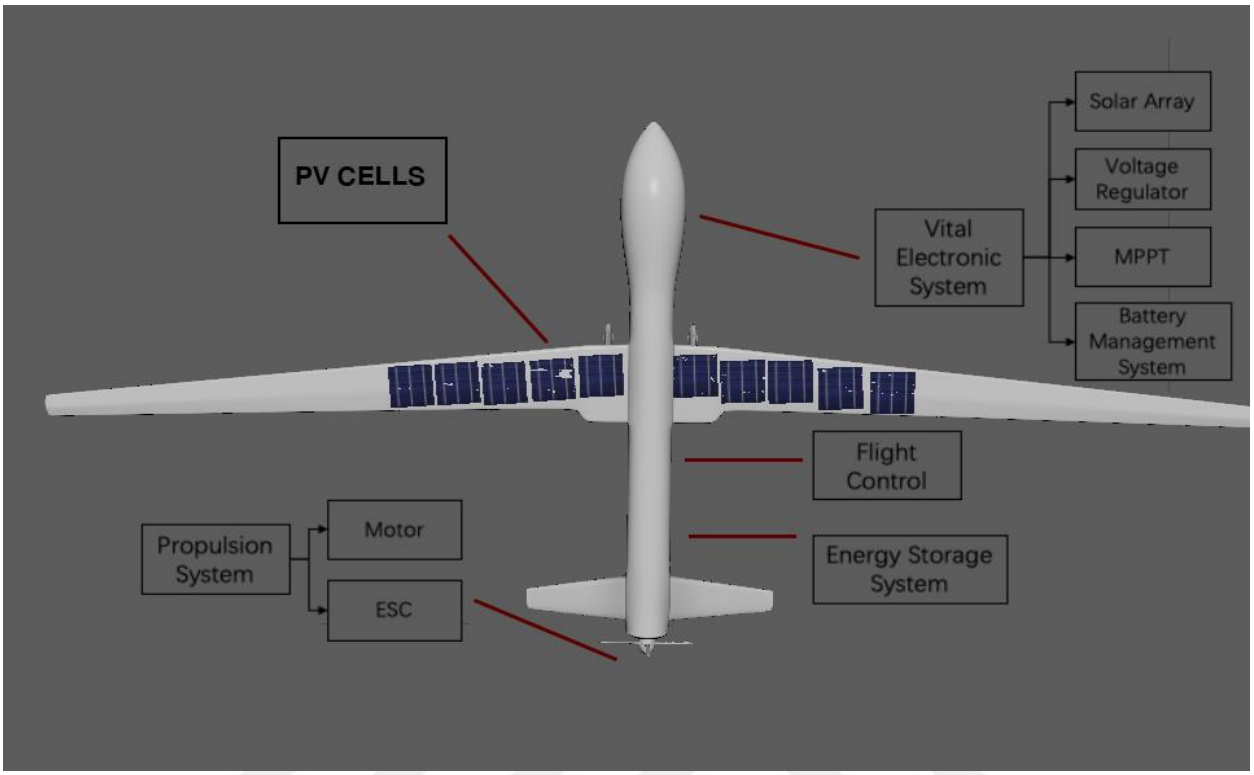

Figure 4.31: Component system if the proposed solar UAV model.

In order to achieve this, the researcher used two methods to improve the travel time of the UAV aircraft: the first was to replace the wing, which improved the travel time due to reduced drag forces, and the second was to add a solar energy resource to feed the engine power and reduce the used fuel content. The energy density of lithium batteries is a critical problem in UAV design. The practical implementation of lithium metal batteries has been delayed due to the formation of dendrites on the surface of the lithium electrode and the difficulties associated with creating an electrolyte with the required mechanical strength and ionic conductivity for solid electrolytes. Although several research institutes and companies are trying to improve energy density with different methods and materials, the energy density of batteries that can be mass produced is still lower than 250Wh/kg at present. Rigorous calculations were required to arrive at the solar cell configuration on the aircraft and the suitable arrangement for the electrical system requirements. The larger the battery capacity also means the larger the solar panel area required for the same charging time, the larger the motor thrust required for flight, and the relationship between them is almost linear. The relationship results in almost all the power

redundancy being consumed by the extra battery weight, making it difficult to allocate the excess power to the payload.

Table 4.10: Numerical Results of UAV Properties.

Model	S1223	S1223 RTL
Wingspan	3m	3m
Wing Area	2.196m	2.196m
min velocity (v)	8.4 m/s	8.2m/s
lift load	233.3388N	240.7633N
UAV weight	20kg	20kg
flight time	8 hrs	8.195hrs
CD	0.047	0.042
P_{total}	749.3835	622.9587

Prior to the flying test, testing must be conducted in order to identify the properties of the solar cells that are installed on the aircraft. There must be a clear sky from 9:30 a.m. to 1:30 p.m. for the testing, and there must be 10 minutes of rest between each data collection. During the flight test, the solar cells that have been mounted on the UAV will be evaluated to assess how well they convert solar energy into usable electricity. By mounting solar panels to the wings of an unmanned aerial vehicle (UAV), its power output may be increased from 150 to 200 watts.

There are three distinct methods for calculating the average amount of current drawn. The first approach is to ascertain the amount of current that is being pulled at a given push, which is information that can only be gained by testing. The second approach involves interpolating the current value using the lowest and maximum currents of the motor, which are represented on the graph of the motor. E-calc was used throughout the last phase of the procedure, which included running simulations on a variety of e-sites. In this situation, the second and third techniques were used, and the resulting estimate was 3.85 amps. Initially, it is envisaged that the length of time spent in the air without a secondary battery unit would not exceed one hour. 7.79 minutes of flight time is 3.60 multiplied by 3.85 multiplied by 6. Once the primary battery is completely charged, the secondary battery will continue to discharge until it can no longer be charged by solar radiation. At this time, the secondary battery will have been entirely exhausted. Given the

conditions, it is impossible to provide an exact estimate of the time required to get from point A to point B. As a result, the worst-case flight duration was computed by assuming that the auxiliary battery would only need to be recharged once (+500mAh) for the whole journey. The flying duration is equal to (3.5 x 60) divided by (3.85 x 6).

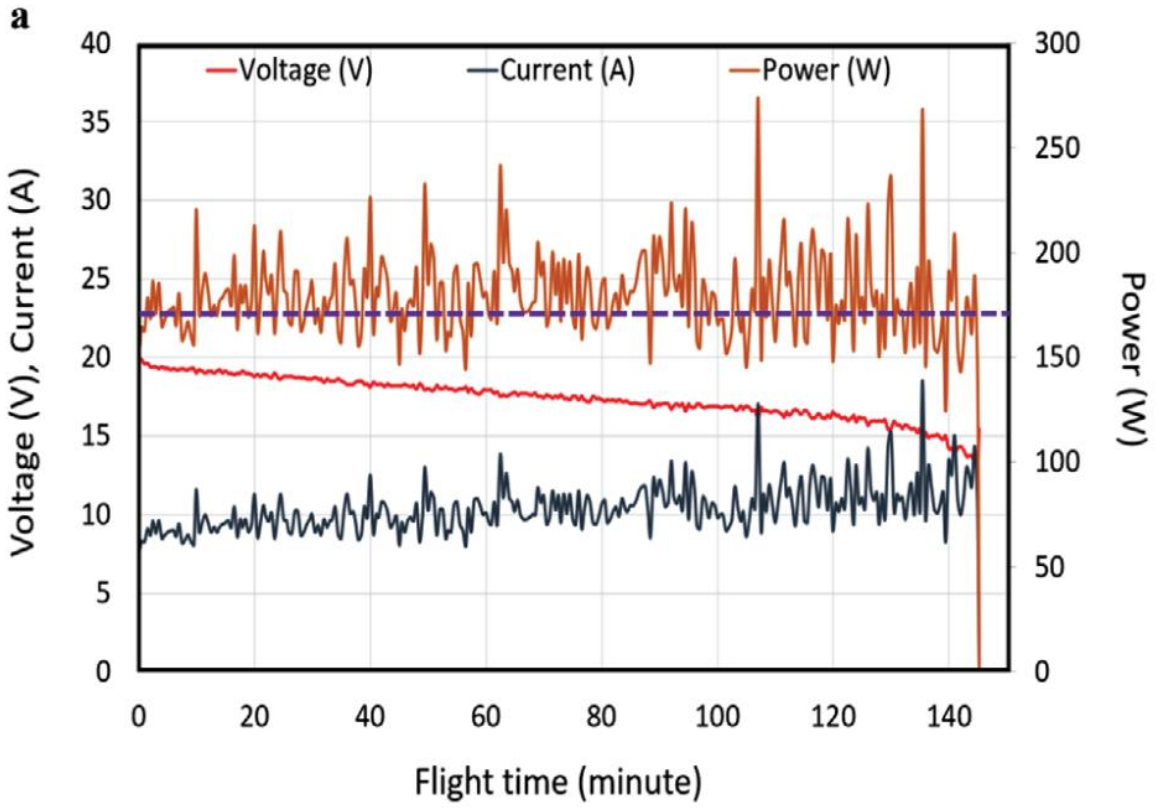

Figure 4.32: flight time after PV optimization.

5. CONCLUSION AND RECOMMENDATION

The methods used in this research addressed some gaps and satisfied the study's goal. The examination of two types of wings is one of the two contributions made in this work. S1223 and S1223 RTL are the two models. The drag and lift coefficients were used in the analysis. The second step is to improve the wing design by including a solar energy power source to increase flying duration. This conclusion was acquired after determining which wings had the best design. The CFD ANSYS program was used as an advanced approach in this study. The lift and drag coefficients are better calculated using the simulation approach used in this thesis.

5.1 CONCLUSIONS

Different turbulence models are observed in the CFD simulation results. According to the research, wing design has a significant impact on aircraft performance. To examine complicated wing correlations, the lift and drag coefficients are used as an aerodynamic number to simulate the complex relationships between shape, flow conditions, and inclinations. The best lift force, according to the study, has to do with the angle of attack in order to minimize drag and lessen the vortex. Based on these data, the performance of the airfoil test results is described as follows:

a) The S1223 CFD ANSYS findings show that the lift force rises progressively as the angle of attack increases, especially between 5^{o} and 10^{o}. This conclusion emphasizes the relevance of the wing's bottom surface form in generating lift force.

b) The features of the air layers around the wing surface influence the air movement behavior, which is altered when air molecules adhere to the wing surface.

c) The values of the lift and drag coefficients increase in a linear progressive manner. The air flow on the wing surface also creates vortex lines that extend from the wing tip and a downwash of air behind the wing.

d) In the S1223 RTL instance, the same phenomena and airfoil characteristics arise. The differing wing designs account for the relative variances in lift force and coefficients.

e) The researchers find that the amount of produced lift is dependent on the geometry of the wing in both circumstances. In the S1223 RTL wing, increasing the area improves the lift force and lift coefficient. The drag coefficient shows the same effect.

f) A downward velocity component in the free stream wing head can be created by the vorticity semi-finite sheet dispersed in the wake.

If solar-powered unmanned aerial vehicles (UAVs) employ dispersed propulsion systems, they may be able to reduce their size while maintaining their endurance. It is conceivable for a distributed propulsion system to save up to 20%-23% of the energy required by a monolithic system to achieve the same amount of lift. When employing a dispersed propulsion system, it is feasible to govern the UAV's propulsion system in either a homogeneous or heterogeneous way, which increases the UAV's mobility. In addition to its improved net power production, double-sided solar panels may be advantageous. By using the underside of the wing, it is feasible to achieve a net energy intake of 43.08w by adding 300 grams of extra mass to the system

5.2 FUTURE WORK AND RECOMMENDATION

The findings reveal a number of recommendations that should be addressed in future research:

a) It is recommended that a wing system with a larger surface area create higher lift forces. This may be accomplished by improving the wing design in terms of both lower surface form and the addition of vortex reducers.

b) To look at the impact of an aircraft's front wing on the tail. This concept may be observed as a novel tail design that reduces the vortex.

REFERENCES

[1] J. Winslow, H. Otsuka, B. Govindarajan, and I. Chopra, "Basic understanding of airfoil characteristics at low Reynolds numbers (104–105)," *J. Aircr.*, vol. 55, no. 3, pp. 1050–1061, 2018, doi: 10.2514/1.C034415.

[2] N. Prajapati, U. Patdiwala, and P. Surani, "Experimental Validation of NACA 6409 Airfoil Using CFD Analysis," vol. 8, no. 4, pp. 0–7, 2021, [Online]. Available: www.jetir.org.

[3] A. C. Zohary, W. Asrar, and M. Aldheeb, "Numerical investigation on the pressure drag of some low-speed airfoils for UAV application," *CFD Lett.*, vol. 13, no. 2, pp. 29–48, 2021, doi: 10.37934/cfdl.13.2.2948.

[4] P. H. Chung, D. M. Ma, and J. K. Shiau, "Design, manufacturing, and flight testing of an experimental flying wing UAV," *Appl. Sci.*, vol. 9, no. 15, 2019, doi: 10.3390/app9153043.

[5] A. Altememe, O. J. Myers, and A. Hall, "Preliminary Design and Computational Fluid Dynamic analysis of Flapping Wing of Micro Aerial Vehicle for Low Reynolds Numbers Regime," *Int. J. Aeronaut. Aerosp. Eng.*, vol. 1, no. 2, pp. 36–45, 2019, doi: 10.18689/ijae-1000106.

[6] N. Aydın, M. Erman Çalışkan, I. Karagoz, and İ. Karagöz, "Numerical Simulation of Flow Over Different Types of Airfoils," no. January, 2020, [Online]. Available: https://www.researchgate.net/publication/338936731.

[7] Y. F. GÖRGÜLÜ, M. A. ÖZGÜR, and R. KÖSE, "NACA 0009 Profilli Bir Kanadin Düşük Bir Reynolds Sayisinda Had Analizi," *J. Polytech.*, vol. 0900, no. 3, pp. 1237–1242, 2021, doi: 10.2339/politeknik.877391.

[8] V. Silkov and A. Zirka, "Calculation of the characteristics of a UAV launch from a ramp," *Aviation*, vol. 18, no. 4, pp. 178–184, 2014, doi: 10.3846/16487788.2014.985476.

[9] N. Rastogi, S. Shetty, and B. Ashok, "Analysing the effects of air flow on a formula

prototype vehicle to optimize its performance," *IOP Conf. Ser. Mater. Sci. Eng.*, vol. 263, no. 6, 2017, doi: 10.1088/1757-899X/263/6/062033.

[10] S. Kandwal and S. Singh, "Computational Fluid Dynamics Study Of Fluid Flow And Aerodynamic Forces On An Airfoil," *Int. J. Eng. Res. Technol.*, vol. 1, no. 7, pp. 1–8, 2012.

[11] L. D. Jathar and S. Borse, "Determination of Coefficient of Lift And Lift Force on Sedan Car Body by Determination of Coefficient of Lift And Lift Force on Sedan Car Body by Changing Different Parameters Using Open Foam," no. September, pp. 9–18, 2019.

[12] C. Pranesh, M. Sivapragasam, M. D. Deshpande, and H. K. Narahari, "Negative lift characteristics of NACA 0012 aerofoil at low Reynolds numbers," *Sadhana - Acad. Proc. Eng. Sci.*, vol. 44, no. 1, pp. 1–6, 2019, doi: 10.1007/s12046-018-1008-6.

[13] H. V. Abeywickrama, B. A. Jayawickrama, Y. He, and E. Dutkiewicz, "Empirical Power Consumption Model for UAVs," *IEEE Veh. Technol. Conf.*, vol. 2018-August, pp. 1–5, 2018, doi: 10.1109/VTCFall.2018.8690666.

[14] E. Bertran and A. Sanchez-Cerda, "On the Tradeoff between Electrical Power Consumption and Flight Performance in Fixed-Wing UAV Autopilots," *IEEE Trans. Veh. Technol.*, vol. 65, no. 11, pp. 8832–8840, 2016, doi: 10.1109/TVT.2016.2601927.

[15] A. De Gaspari and F. Moens, "Aerodynamic shape design and validation of an advanced high-lift device for a regional aircraft with morphing droop nose," *Int. J. Aerosp. Eng.*, vol. 2019, 2019, doi: 10.1155/2019/7982168.

[16] T. A. Shams, S. I. Ali Shah, A. Javed, and S. H. R. Hamdani, "Airfoil selection procedure, wind tunnel experimentation and implementation of 6DOF modeling on a flyingwing micro aerial vehicle," *Micromachines*, vol. 11, no. 6, pp. 1–31, 2020, doi: 10.3390/MI11060553.

[17] R. Islam Rubel, M. Kamal Uddin, M. Zahidul Islam, and M. Rokunuzzaman, "Numerical and Experimental Investigation of Aerodynamics Characteristics of NACA 0015 Aerofoil," *Int. J. Eng. Technol. IJET*, vol. 2, no. 4, pp. 132–141, 2017, doi:

10.19072/ijet.280499.

[18] M. Anyoji, “High-performance airfoil with low reynolds-number dependence on aerodynamic characteristics,” *Fluid Mech. Res. Int. J.*, vol. 3, no. 2, pp. 76–80, 2019, doi: 10.15406/fmrij.2019.03.00055.

[19] P. Manuel and C. Aleixo, “Design and Testing an Experimental UAV Engenharia Aeroespacial,” p. 65, 2007.

[20] S. Iswahyudi, Sutrisno, Prajitno, and S. B. Wibowo, “Airfoil types effect on geometry and performance of a small-scale wind turbine blade design,” *J. Appl. Eng. Sci.*, vol. 18, no. 1, pp. 132–139, 2020, doi: 10.5937/jaes18-23413.

[21] T. Kamas, “2-D and 3-D Assessment of Cambered and Symmetric Airfoils : a Cfd Study,” no. December, 2009.

[22] M. Zakaria, M. Abdallah, and M. Elshafie, “Design and Production of Small Tailless Unmanned Aerial Vehicle,” *Int. Conf. Appl. Mech. Mech. Eng.*, vol. 15, no. 15, pp. 1–26, 2012, doi: 10.21608/amme.2012.36970.

[23] Y. H. Irawan, E. Yawara, and H. Bakhtiar, “Effect of Tapper Ratio on a Car Rear Spoiler Performance,” vol. 4, no. 1, pp. 1–14, 2019.

[24] R. H. Barnard and D. R. Philpott, *Mechanics*. .

[25] M. F. Ur Rab and M. J. Alam, “Comparative analysis of high-lift airfoils for motorsports applications,” *WIT Trans. Eng. Sci.*, vol. 120, no. April 2019, pp. 17–183, 2018, doi: 10.2495/AFM180171.

[26] Sumit Sharma, “An Aerodynamic Comparative Analysis of Airfoils for Low-Speed Aircrafts,” *Int. J. Eng. Res.*, vol. V5, no. 11, pp. 525–529, 2016, doi: 10.17577/ijertv5is110361.

[27] M. M. Rubiat Mustak,Md.Harun-Or-Rashid Molla, “Improvement of Aerodynamic Characteristics of an Airfoil by Surface Modification,” *Am. J. Eng. Res.*, vol. 6, no. 3, pp. 07–14, 2017, [Online]. Available: http://www.ajer.org/papers/v6(03)/B06030714.pdf.

[28] T. D. Ipilakyaa, L. T. Tuleun, and M. O. Kekung, “Computational fluid dynamics modelling of an aerodynamic rear spoiler on cars,” *Niger. J. Technol.*, vol. 37, no. 4, p. 975, 2018, doi: 10.4314/njt.v37i4.17.

[29] Y. Wang, X. Lyu, H. Gu, S. Shen, Z. Li, and F. Zhang, “Design, implementation and verification of a quadrotor tail-sitter VTOL UAV,” *2017 Int. Conf. Unmanned Aircr. Syst. ICUAS 2017*, no. June, pp. 462–471, 2017, doi: 10.1109/ICUAS.2017.7991419.

[30] H. H. Hurt Jr., “Aerodynamics for Naval Aviators,” *Citeseer*, no. January, 1965.

[31] V. G. Pathade, K. B. Kale, and S. K. More, “CFD Analysis & Experimental investigation of NACA0018 Blade Profile for Darrieus Turbine,” vol. 4, no. 8, pp. 1–9, 2016.

[32] S. Bezavada and S. P. Kodali, “Numerical simulation of air flow over a passenger car and the Influence of rear spoiler using CFD,” *Int. J. Adv. Transp. Phenom.*, vol. 01, no. 01, 2012, [Online]. Available: https://www.researchgate.net/publication/336589740.

[33] Federal Aviation Administration, “Aerodynamics of Flight,” *Pilot. Handb. Aeronaut. Knowl.*, no. Cl, pp. 2–5, 2000.

[34] A. T. P. Helo and F. Cfii, “Airfoil performance monitor Advanced technology offers new defense against persistent challenges to safe all-weather flight . PILOT ADVISORY DEVICES,” no. March, pp. 2–4, 2011.

[35] S. Sharma, “Airfoil Terminology , Its Theory and Variations As Well As Relations with Its Operational Lift Force and Drag Force in Ambient Conditions,” vol. 2, no. 1, pp. 268–277, 2015.

[36] B. E. Har and M. E. June, “Numerical Investigation on the Aerodynamic Gliding Performance of an Ornithopter,” no. June, 2017.

[37] G. K. W. Kenway and J. R. R. A. Martins, “Multipoint High-Fidelity Aerostructural Optimization of a Transport Aircraft Configuration,” *J. Aircr.*, vol. 51, no. 1, pp. 144–160, 2014, doi: 10.2514/1.C032150.

[38] K. Lawrence *et al.*, *Modeling and Finite Element Analysis*, vol. 019. 2019.

[39] R. Lanzafame, S. Mauro, and M. Messina, “Evaluation of the radial flow effects on micro HAWTs through the use of a transition CFD 3D model - Part II: Postprocessing and comparison of the results,” *Energy Procedia*, vol. 82, pp. 164–171, 2015, doi: 10.1016/j.egypro.2015.12.013.

[40] M. A. F. Kandil and A. Okasha Elnady, “Performance of GOE-387 Airfoil Using CFD,” *Int. J. Aerosp. Sci.*, vol. 2017, no. 1, pp. 1–7, 2017, doi: 10.5923/j.aerospace.20170501.01.

[41] H. W. Park and W. B. Yoon, “Computational fluid dynamics (CFD) modelling and application for sterilization of foods: A review,” *Processes*, vol. 6, no. 6, 2018, doi: 10.3390/pr6060062.

[42] M. Anyoji, “High-performance airfoil with low reynolds-number dependence on aerodynamic characteristics,” Fluid Mech. Res. Int. J., vol. 3, no. 2, pp. 76–80, 2019, doi: 10.15406/fmrij.2019.03.00055.

[43] Betancourth, N. J. P., Villamarin, J. E. P., Rios, J. J. V., Bravo-Mosquera, P. D., & Cerón-Muñoz, H. D. (2016). Design and manufacture of a solar-powered unmanned aerial vehicle for civilian surveillance missions. Journal of Aerospace Technology and Management, 8(4), 385–396. https://doi.org/10.5028/jatm.v8i4.678

[44] Lussier, M. E., Detweiler, C., & Bradley, J. (2019). Extending endurance of multicopters: The current state-of-the-art. AIAA Scitech 2019 Forum. https://doi.org/10.2514/6.2019-1790

[45] Lussier, M. E., Detweiler, C., & Bradley, J. (2019). Extending endurance of multicopters: The current state-of-the-art. AIAA Scitech 2019 Forum. https://doi.org/10.2514/6.2019-1790

[46] Betancourth, N. J. P., Villamarin, J. E. P., Rios, J. J. V., Bravo-Mosquera, P. D., & Cerón-Muñoz, H. D. (2016). Design and manufacture of a solar-powered unmanned aerial vehicle for civilian surveillance missions. Journal of Aerospace Technology and Management, 8(4), 385–396. https://doi.org/10.5028/jatm.v8i4.678